FINAL REPORT

On-Command Pyrotechnic Light Emission Through Controlled Electromagnetic Irradiation

WP19-C4-1163

Jonathan Dilger, Eric Miklaszewski, William Crespo
Naval Surface Warfare Center (NSWC), Crane Division
300 Highway 361, Crane, IN 47522-5001
Ph: 812-854-1452, E: jonathan.m.dilger@navy.mil

Travis Sippel, James Michael, Shankar Subramaniam
Iowa State University

Performance Period: 28th June 2019 – 1st October, 2020

1st October, 2020

REPORT DOCUMENTATION PAGE

Form Approved
OMB No. 0704-0188

1. REPORT DATE *(DD-MM-YYYY)*	**2. REPORT TYPE**	**3. DATES COVERED** *(From - To)*
01/10/2020	SERDP Final Report	6/28/2019 - 10/1/2020

4. TITLE AND SUBTITLE

On-Command Pyrotechnic Light Emission Through Controlled Electromagnetic Irradiation

5a. CONTRACT NUMBER

5b. GRANT NUMBER

5c. PROGRAM ELEMENT NUMBER

6. AUTHOR(S)

Jonathan Dilger, Eric Miklaszewski, and Stuart Barkley
Naval Surface Warfare Center (NSWC), Crane Division

William Crespo
Naval Research Laboratory

Travis Sippel, James Michael, and Shankar Subramaniam
Iowa State University

5d. PROJECT NUMBER
WP19-1163

5e. TASK NUMBER

5f. WORK UNIT NUMBER

7. PERFORMING ORGANIZATION NAME(S) AND ADDRESS(ES)
Naval Surface Warfare Center (NSWC), Crane Division
300 Highway 361
Crane, IN 47522-5001

8. PERFORMING ORGANIZATION REPORT NUMBER
WP19-1163

9. SPONSORING/MONITORING AGENCY NAME(S) AND ADDRESS(ES)
Strategic Environmental Research and Development Program (SERDP)
4800 Mark Center Drive, Suite 16F16
Alexandria, VA 22350-3605

10. SPONSOR/MONITOR'S ACRONYM(S)
SERDP

11. SPONSOR/MONITOR'S REPORT NUMBER(S)
WP19-1163

12. DISTRIBUTION/AVAILABILITY STATEMENT

DISTRIBUTION STATEMENT A. Approved for public release: distribution unlimited.

13. SUPPLEMENTARY NOTES

14. ABSTRACT

The aim of this effort is to experimentally and computationally explore the effects of microwave irradiation on light emission from pyrotechnic flames within free-space microwave fields. Recent efforts have shown that microwave illumination of pyrotechnic flames can result in effects such as dynamic amplification of luminosity and shifting of flame chromaticity. However, the underpinnings of the interaction of high frequency electric fields with plumes from pyrotechnic formulations remain unknown.

15. SUBJECT TERMS

Pyrotechnic Light Emission, Controlled Electromagnetic Irradiation

16. SECURITY CLASSIFICATION OF:			**17. LIMITATION OF ABSTRACT**	**18. NUMBER OF PAGES**	**19a. NAME OF RESPONSIBLE PERSON**
a. REPORT	**b. ABSTRACT**	**c. THIS PAGE**			Jonathan Dilger
UNCLASS	UNCLASS	UNCLASS	UNCLASS	56	**19b. TELEPHONE NUMBER** *(Include area code)* 812-854-1452

Table of Contents

Contents

Abstract 8
Executive Summary 9
Objective 10
Background 10
Microwave Enhancement of Emission in Alkali-Containing Pyrotechnics 11
MW Emission Color Shifting in Mg/PTFE Pyrotechnics 15
Materials and Methods 17
Equilibrium Calculations 17
Pyrotechnic Formulation and Manufacture 17
Boron Propellant Formulation and Manufacture 18
Microwave Combustion Cavities 18
Free-Space Microwave Cavity 18
Multi-Mode Cavity 20
Premixed, Seeded Burner 21
Combustion Diagnostics 23
Experimental Data Post-Processing 23
Time-Integrated, Total Emission, Chromaticity, and Luminosity 23
Continuum Temperature Calculation 24
Computational Methods 25
1. Microwave-Enhanced (VIS/NIR) Alkali Emission Model 27
2. Electron Kinetics in Microwave Combustion & Boltzmann Equation Solutions 30
3. Non-Equilibrium Microwave-Enhanced Reacting Flow Models 31
Results and Discussion 32
Exploration of the Effect of Free Electron Concentration on Field-Flame Coupling in a Free-Space E-Field 32
Effect of Variation of Mg/PTFE Stoichiometry on Emission in a Free-Space E-Field 36
Plasma Modeling Using Monte-Carlo Methods 39
Modeling of the Microwave Enhancement of Light Emission from a Mg/NaNO3 Pyrotechnic Flame 40
Microwave Interaction with Ba-Doped Mg/PTFE Pyrotechnics in a Free-Space E-Field 43
Boron Combustion 44

Development of Gas-Phase, Premixed Particle-Seeded Burner for Microwave Interaction Studies 47
Conclusions, Future Research Directions and DoD Implications 49
Literature Cited 53
Appendices 55
Scientific / Technical Publications 55

Listing of Tables

Table 1. Formulations experimentally investigated. 17

Table 2. Fuel-rich boron propellant formulations and corresponding equilibrium performance. 18

Listing of Figures

Figure 1. Image sequence of the Mg/KNO_3/epoxy pyrotechnic combustion with (top) and without (bottom) microwave illumination, where the microwave field is sinusoidally modulated at 60 Hz. During the microwave illumination period, flame growth and emission increase can be seen above the main flame. Both images are taken with the same exposure and frame rate (20 μs, 500 Hz). 11

Figure 2. Image sequence of the microwave field enhancement of Mg/$NaNO_3$/epoxy post-combustion products where the microwave field is sinusoidally modulated at 60 Hz. The pyrotechnic article is out of view in these images. 12

Figure 3. (a) Time-integrated, relative spectral irradiance of each pyrotechnic during combustion, both with and without microwave illumination in arb. units per gram pyrotechnic reagent. Species responsible for strong electronic transition features observed in VIS/NIR emission are noted. Increased emission from atomic transitions can be seen with illumination. Some atomic emission enhancement is also observed from contaminant alkali species that are present in the multimode microwave cavity which are excited during combustion and microwave illumination (e.g. Li, Na, K, and Cs). Spectra intensities are all relative and spectra from each formulation are offset for clarity. (b) Typical emission spectral features from Mg/$NaNO_3$/epoxy pyrotechnic combustion with and without microwave. 13

Figure 4. CIE 1931 chromaticity diagram showing time-resolved color and purity of emission from Mg/$NaNO_3$/epoxy pyrotechnics (1) without microwave illumination, (2) with microwave illumination, and (3) emission acquired from microwave illumination of combustion products post-extinguishment. Graybody emission at 2725 K and the Illuminant E point is indicated on the diagram. The dash line represents dominant wavelength of 589.2 nm of varying color purity. .. 14

Figure 5. Time-integrated, infrared total spectral irradiance of each Mg/alkali nitrate/epoxy pyrotechnic with and without microwave illumination. Species of significant electronic atomic and molecular emission enhancements observed are noted. Irradiance values for each formulation are offset for presentation purposes. 15

Figure 6. Color image sequences of Mg/PTFE combustion taken with (top) and without (bottom) microwave illumination. Both image sequences have the same camera settings (200 Hz, 4 μs). 16

Figure 7. (a) Time-integrated UV/VIS/NIR emission spectra from Mg/PTFE combustion with and without microwave illumination (averages of three tests). Also shown is the post-combustion emission from the pyrotechnic (time-integrated from one trial). Spectra are offset for presentation. (b) Normalized time-integrated and wavelength-integrated total UV/VIS/NIR irradiance (260 nm to 900 nm) of Mg/PTFE emission with and without microwave illumination. Reported values and error bars represent the averages and standard deviations of three experimental trials each. 16

Figure 8. Left: Photo of free-space microwave combustion cavity. Right: Diagram of free-space combustion cavity. Diagnostics observe the combustion plume from the sized through access door through a faraday cage (not shown). 19

Figure 9. Left: COMSOL simulation of E-field distribution within the free-space cavity using an open waveguide (no antenna) condition. Simulated electric field strength as a function of distance along the centerline of the cavity. The output power of the antenna port was set to 2 kW. 20

Figure 10. Power loss (S_{21}) as a function of distance away from an open waveguide port (WR-284) in the free space cavity. COMSOL Multiphysics was utilized to compared measured values, in which an average power loss was calculated by matching the receiving antenna cross-sectional area. 20

Figure 11. (a) Schematic of the experimental setup of the microwave cavity. Experiments were monitored with a color high-speed camera and two spectrometers (VIS/NIR and IR). (b) Distribution of the mean electric field strength simulated using COMSOL within the microwave chamber. The red circle indicates the location of the pyrotechnic flame, which is located at an E-field antinode with an average field strength of 2.1 ± 0.1 kV/m in a 100 cm^3 volume of water.. 21

Figure 12. Disassembled premixed gas-phase burner including the top "cap" of the burner (a) the gas mixing chamber section (b) with external threads to mate with the top and the base with the particle feeding tube (c) attached, where the premixed gases enter laterally into the burner. 22

Figure 13. An example of the MATLAB GUI used to evaluate the condensed-phase combustion temperature by fitting of continuum emission regions (650 – 750 and 775-825 nm shown) to a graybody curve. 25

Figure 14. Project tree for modeling microwave-enhanced combustion and emission, relevant for pyrotechnic plumes and seeded flames. Milestones broken down into combustion models, electron kinetics, electron fluid models, and radiation-transfer models, which synthesis in integrated models is being developed. 26

Figure 15. Example configuration of the homogenous plume model with an incident electric field propagating left to right, perpendicular to the plume surface. Radiance is computed at surface, $s = 0$, simulating light available for detection. 28

Figure 16. (Left) Electron collision rates in atmospheric gas relative to field frequency (right) Monte Carlo benchmarks for attachment compared to BOLSIG+ simulations 31

Figure 17. CEA simulation of a 1/1 wt. ratio Mg/PTFE pyrotechnic with addition of $NaNO_3$. .. 33

Figure 18. Color image sequences of the combustion plume from Mg/PTFE doped with indicated quantities of $NaNO_3$. Combustion occurs within a free space microwave field with application of field (bottom) and without field application (top). Images are all taken with the same exposure (10 μs) and aperture settings. The free space field was generated from an open waveguide with a 2 kW magnetron. 34

Figure 19. Total integrated emission of 1/1 wt. ratio Mg/PTFE pyrotechnic expose to a microwave field as a function of $NaNO_3$ addition. a) 0 wt.% $NaNO_3$, b) 0.1 wt.% $NaNO_3$, c) 0.5 wt.% $NaNO_3$, d) 5 wt.% $NaNO_3$. 35

Figure 20. CIE 1931 color space diagram of a 1/1 wt. ratio Mg/PTFE with 0.1 wt.% $NaNO_3$ addition. Blue dash line represents a black body emitter from 1000K to 5000K. 36

Figure 21. Color images of Mg/PTFE combustion within a free space microwave field (bottom) and without a field (top). Images are taken with the same exposure (10 μs), aperture settings, and a neutral density filter (OD 1.2). The free space field was generated from an open waveguide with a 2 kW magnetron. 37

Figure 22. Emission spectra of Mg/PTFE combustion with and without a microwave field (free space field). Formulation are the following: (a) 35/65 wt. Mg/PTFE, (b) 50/50 wt. Mg/PTFE, and (c) 65/35 wt. Mg/PTFE. 37

Figure 23. Example fitting of MgO $B^1\Sigma$ -$X^1\Sigma$ ($\Delta v=0$) emission spectra and temperature fitting of the simulated transition. 38

Figure 24. MgO rotational-vibrational gas-phase temperatures of Mg/PTFE combustion (50/50 wt. ratio left, 65/35 wt. ratio right) with and without microwave from two pyrotechnics experiments within a 2.45 GHz free-space microwave field of 30 kV/m. 39

Figure 25. BOLSIG+ and Monte Carlo predictions of mean energy across a representative methane-air flame. Axial mixture and temperature were computed using Cantera. 40

Figure 26. (a) Model results for ratio of radiance with and without applied microwave is shown (Eqn. 14). A best fit solution was found for incident RMS field strength of 42 Td, alkali mole fraction of 6 vol.%, and temperature of 2725 K (blue). A high temperature case representative of CEA equilibrium conditions is also shown (red). Each case is plotted at line center $\lambda 21$, with perturbations in wavelength showing the local sensitivity from several terms in Eqn. 3-15 producing positive change with wavelength ($\lambda +$) , the single term $KM +$ producing negative change ($\lambda -$), and total change ($\lambda - \ and \ \lambda +$). Experimental frequency-integrated irradiance ratios are also plotted, with error bars representing the standard deviation of three trials (green). Lastly, a set of eight simulations are shown covering the practical limits across the three major parameters (gray). (b) The enhancement ratio in (a) is computed for sodium over a range of temperature and field strength values. Contours representing the corresponding experimental value plus/minus one standard deviation are overlaid with simulations, along with the fitted temperature and field strength. 42

Figure 27. Emission spectra of 47.25/47.25/5 wt. % Mg/PTFE/$Ba(NO_3)_2$ combustion with and without a microwave field (free space field). 43

Figure 28. Chromaticity diagram showing dominant emission color of $Ba(NO_3)_2$-doped (5 wt.%) Mg/PTFE pyrotechnic flames both with and without microwave illumination. Microwave illumination is from a 2 kW magnetron source within a free-space cavity. 44

Figure 29. a) Time-resolved spectra of a 30 wt% boron propellant without (left) and with (right) microwave irradiation. b) Time-averaged BO_2 emission and c) time-averaged total emission(400 to 850 nm) for boron (B) and boron carbide (BC) propellant formulations both with and without microwave irradiation. Percentages indicate the degree of emission enhancement as compared to the same formulation without MW. 45

Figure 30. Average burning rate across three trials for each formulation. Enhancement due to microwave irradiation shown in percent above each formulation. Error bars indicate one standard deviation of all measurements. 46

Figure 31. Computed graybody temperature measurement from propellant flames with and without microwave irradiation. Values are averages and error bars indicate one standard deviation of all measurements. 47

Figure 32.Image of premixed particle-seeded gas burner stable flame condition without seeding (left) and with boron particle seeding (right). 48

Abstract

The aim of this effort is to experimentally and computationally explore the effects of microwave irradiation on light emission from pyrotechnic flames within free-space microwave fields. Recent efforts have shown that microwave illumination of pyrotechnic flames can result in effects such as dynamic amplification of luminosity and shifting of flame chromaticity. However, the underpinnings of the interaction of high frequency electric fields with plumes from pyrotechnic formulations remain unknown. To explore these mechanisms, pyrotechnic articles are burned under the illumination of 2.45 GHz electric fields of ~10 to 50 kV/m. A number of unique light emission effects are observed from atomic flame species (Cs, K, Na), diatomics (BaF, MgF, MgO), and triatomics (BO_2). The ability to microwave modulate flame light emission by as much as ~300 to 400%, the ability to drastically alter pyrotechnic light emission color and flame volume through microwave illumination of formulations containing small quantities (up to 5 wt.%) of additives, among other findings are discussed. A number of steps are taken toward the goal of development of a 2D, transient models capturing combustion chemistry, plasma kinetics, species advection, field propagation, and optical emission on both the electronic timescale (nanoseconds) and the advective timescale (microseconds). Of particular note, the development of a 1D steady state model of high alkali content pyrotechnic combustion indicates that for atomic alkali emitter species, the degree of microwave-induced light emission enhancement is optimized for conditions of low flame temperature and high field strength. Contrary to intuition, alkali atomic emission enhancement is also found to be more favorable at lower wavelengths (higher energy). These results are found to be consistent with experimental measurements. The effort also discusses development of a gas-phase, premixed, particle-seeded burner which will be used to perform studies of light emission augmentation under more controlled flame conditions. The implications of these findings on important future research directions as well as potential DoD applications in development of next generation, 'smart' pyrotechnics and improvement of environmental and toxicological impacts of pyrotechnics are discussed.

Executive Summary

Introduction. Development of next generation pyrotechnic emitters with dynamic, on-command selectable light emission characteristics requires a shift away from the "emission control exclusively via formulation" practice that is effective for passive emitter design. High-brilliance pyrotechnic emitters have also traditionally required addition of toxicological and environmentally harmful additives in order to achieve necessary color purity and brilliance. A number of studies have been previously conducted on microwave emission stimulation within a multimodal microwave cavity that demonstrate that with pyrotechnic flames containing weakly ionized species, microwave field irradiation can produce a 'shift' in light emission color, whereas in pyrotechnic flames containing strongly ionized species (i.e. flames with a high electron population), microwave field irradiation produces light amplification without color shift.

Objectives. The objective of the proposed effort is to develop on-command microwave-selectable color and intensity emissions within a single pyrotechnic formulation by exploiting electromagnetic-flame interactions. The development of this technology will enable tunable, multi-color, and multi-purpose pyrotechnics, where environmental impact could be achieved via (1) reductions in size/weight of ordnance to produce desired photoemission impulse, (2) reduced inventories due to multi-purpose use, and (3) the ability to produce spectral photoemission from environmentally friendly formulations that, without microwave irradiation, are incapable of satisfying photoemission color purity/intensity requirements or through minimization of the use of environmentally harmful and toxicologically harmful additives. Additionally, all prior

Technical Approach. This effort studies the microwave amplification of pyrotechnic light emission through combined experimental and computational approaches. Experiments are conducted on small pyrotechnic articles in free-space and multimodal microwave fields. Computational efforts have led to the development of a suite of capabilities capable of predicting the degree of microwave-induced light emission enhancement occurring from pyrotechnics. Additionally, a premixed, gas-phase, particle seeded burner has been developed that will be utilized in later studies to establish greater control over experimental conditions and to validate modeling efforts.

Results and Discussion. Efforts have demonstrated that microwave light emission enhancement can be extracted from a number of pyrotechnic formulations illuminated by a free-space microwave field and a number of different effects have been demonstrated. Notably, it was shown that using a small quantity of alkali dopant (up to 5 wt.%) in a Mg/PTFE pyrotechnic, one can drastically alter the time-stability of microwave enhancement, the chromaticity of the pyrotechnic flame, and the type of effect microwave illumination has on the pyrotechnic (luminosity enhancement or color switching), suggesting that many different colors and light emission characteristics may be possible from a single pyrotechnic formulation having small changes in type and quantity of dopant addition. High degrees of light amplification of 300% to 400% were found to be possible in boron containing formulations. Modeling capabilities have been developed toward the eventual goal of 2D transient simulation of microwave modulated pyrotechnic emission. A 1-D model of electric field-modified pyrotechnic light emission was developed, from which several discoveries were made. The model indicates electromagnetic shielding in high electron population flames can be significant. The model also shows, counterintuitively, that atomic transitions of lower wavelength (higher energy) produce a greater degree of light intensity modulation. Degree of light amplification is found to optimize at higher field strength and for flames of lower flame temperature.

Implications for Future Research and Benefits. Taken together, these results mitigate much risk associated with pursuit of dynamic control of pyrotechnic light emission with electromagnetic fields, though additional study is necessary. The concurrent development of modeling capabilities is critical to understanding microwave enhanced emission, optimizing processes, would be helpful in application, and is also useful to the design of traditional, non-microwave enhanced pyrotechnics. A number of applications have been identified from this effort, which are described in detail within the Research and Discussion section and are summarized in the Conclusions section.

Objective

The objective of the proposed effort is to develop on-command microwave-selectable color and intensity emissions within a single pyrotechnic formulation by exploiting electromagnetic-flame interactions. The development of this technology will enable a tunable, multi-color, multi-purpose pyrotechnic, simplifying manufacturing and inventory complexities and increasing the utility of pyrotechnic load-outs through multi-use. Additionally, environmental impact could be reduced via (1) reductions in size/weight of ordnance to produce desired photoemission impulse, (2) reduced inventories due to multi-purpose use, and (3) the ability to produce spectral photoemission from environmentally friendly formulations that, without microwave irradiation, are incapable of satisfying photoemission color purity/intensity requirements.

This project aims to improve the understanding of microwave absorption to enable control of light output enhancement from selected chemistries, enabling on-command tuning of flame color and brightness. Research efforts in this one-year project have focused on fundamental mechanisms of microwave coupling with binary and low-level doped binary pyrotechnic systems investigated via both experimental and computational investigations.

The aims of experimental efforts have been to (1) investigate, within a free space environment, the previously observed pyrotechnic light emission enhancement observed in a multimodal microwave cavity resonator; (2) investigate light emission enhancement on additional pyrotechnic formulations, and (3) experimentally inform the understanding of pyrotechnic light emission enhancement (transport, chemical kinetics, and electron kinetics) through a) pyrotechnic experiments and b) the development of a gas-phase, premixed particle-seeded burner to be utilized to make experimental measurements in a more controlled environment.

The aims of computational studies have been to (1) develop a suite of tools for simulating the interaction of alternating electric fields with pyrotechnic plumes, including simulation of chemical/electron kinetics and transport, field propagation, and optical emission, (2) understand the underlying mechanisms of electric field modulated light emission enhancement and the potential for light emission enhancement. These tools are also relevant to pyrotechnic flames in absence of an electric field and are an update to the seminal modeling efforts of the 1970's by BE Douda.

Background

It has been shown that one can readily deposit energy from microwaves directly to the flame of a pyrotechnic or solid propellant, resulting in unique light emission characteristics, flame structure growth, increased non-LTE flame temperatures, and generation of weak plasmas, enhanced burning rate, and sustainment of light emission with field application long after pyrotechnic extinguishment.1 The mechanism through which optical light emission occurs involves absorption of microwave energy by the pyrotechnic plume by a number of mechanisms including (1) electron acceleration and collision with neutrals, (2) dielectric absorption by condensed phase species within the flame (e.g. metal oxides) and enhanced continuum emission, and (3) loss to conductive species (e.g. metals) through eddy current and Maxwell-Wagner microwave energy loss.

At the outset of this project, electric field-moderated light emission enhancement had been observed in a number of different pyrotechnics, including magnesium with oxidizers of alkali

nitrates (cesium, potassium, and sodium), and PTFE. Observations of these light emission enhancements were conducted within both multimodal and single-mode, resonant microwave cavities. In general, two important findings were observed from these studies: 1) in flames containing alkali metals, application of an alternating electric field led to amplification of the pyrotechnic luminosity without change in flame color (chromaticity), and 2) in Mg/PTFE flames, application of an alternating electric field led to significant amplification of blue emission. Following are summaries of the findings of these studies on Mg/alkal nitrate and Mg/PTFE pyrotechnic compositions.

Microwave Enhancement of Emission in Alkali-Containing Pyrotechnics

Effects of MW Frequency E-Field on Flame Structure and Emission. Image sequences (Fig. 1) show an example of the effect of modulated microwave illumination on the flame structure of a Mg/KNO_3/epoxy pyrotechnic. The emission enhancement of the flame is expected, in part, from the high alkali metal content of the formulations, which results in emission from low-lying electronic states [1–5]. For formulations containing nitrates of cesium, potassium, or sodium,, microwave field application increased both the visible flame volume and emission intensity. Additionally, sustained visible light emission after pyrotechnic flame extinguishment was also observed as a result of continued microwave field application. The resulting post-combustion emission, shown in Fig. 2, occurs near the top of the multimodal cavity at a probable E-field antinode. The post-combustion products continue to emit for long durations of time (~10 s or longer after pyrotechnic extinguishment).

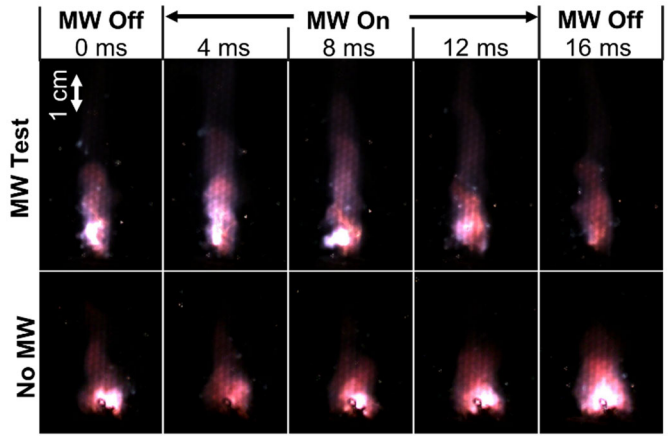

Figure 1. Image sequence of the Mg/KNO_3/epoxy pyrotechnic combustion with (top) and without (bottom) microwave illumination, where the microwave field is sinusoidally modulated at 60 Hz. During the microwave illumination period, flame growth and emission increase can be seen above the main flame. Both images are taken with the same exposure and frame rate (20 μs, 500 Hz).

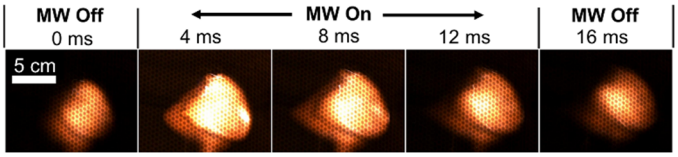

Figure 2. Image sequence of the microwave field enhancement of Mg/$NaNO_3$/epoxy post-combustion products where the microwave field is sinusoidally modulated at 60 Hz. The pyrotechnic article is out of view in these images.

Measurement of time-integrated light emission are computed from light emission measurements from Mg/alkali nitrate pyrotechnics. These results are summarized in time-integrated, VIS/NIR spectral irradiance measures of the three pyrotechnic formulations (Fig.3). The majority of emission enhancement observed in all pyrotechnic formulations was due to enhanced emission from low energy electronic transitions from excited state alkali neutrals. As expected, resonant broadening and self-absorption of the alkali resonance-line continuum is apparent (Fig. 3b) without microwave illumination. Self-absorption also occurs in microwave illuminated emission from all formulations, though is not apparent in time-integrated spectra of Fig. 3a due to the additional emission contribution of the microwave-supported plasma that occurs after pyrotechnic extinguishment.

For pyrotechnic formulations investigated, microwave energy is expected to be preferentially absorbed electronically to the gas-phase through inelastic electron-neutral collisions rather than dielectrically by the condensed-phase reactants. Some dielectric heating of the condensed phase does occur, however, as demonstrated by microwave-based auto-ignition of pyrotechnic articles which can be achieved after ~40 seconds of microwave illumination. Assuming pyrotechnic article microwave heating is spatially uniform and assuming autoignition occurs between 467 °C and 565 °C [6], and neglecting convective losses, we estimate the average microwave absorption of condensed phase reactants is 6.0 W to 7.3 W. Much of the condensed phase reactant heating is expected to be a result of microwave loss in the metal nitrate.

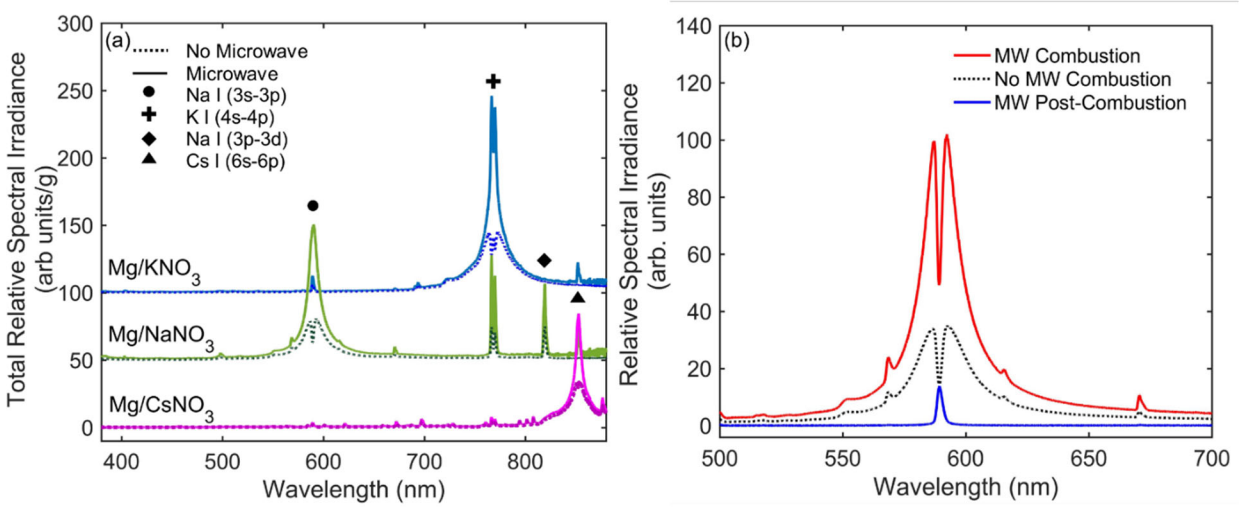

Figure 3. (a) Time-integrated, relative spectral irradiance of each pyrotechnic during combustion, both with and without microwave illumination in arb. units per gram pyrotechnic reagent. Species responsible for strong electronic transition features observed in VIS/NIR emission are noted. Increased emission from atomic transitions can be seen with illumination. Some atomic emission enhancement is also observed from contaminant alkali species that are present in the multimode microwave cavity which are excited during combustion and microwave illumination (e.g. Li, Na, K, and Cs). Spectra intensities are all relative and spectra from each formulation are offset for clarity. (b) Typical emission spectral features from Mg/$NaNO_3$/epoxy pyrotechnic combustion with and without microwave.

Microwave Effects on Luminosity and Chromaticity. Emission from the Mg/$NaNO_3$/epoxy time-series spectra were plotted on chromaticity diagrams (Fig. 4) for three conditions: baseline pyrotechnic combustion without microwave illumination, pyrotechnic combustion with microwave illumination, and microwave illumination of post-combustion products. Fig. 4 shows high color purity for all three conditions. Emission for all three conditions is dominated by the 589 nm Na I emission (3p-3s transition, Fig. 3) and Fig. 4 further shows that all three conditions produce light emission of similar dominant wavelength. With respect to the subtle trends in emission, with microwave illumination, emission becomes more monochromatic and follows the 589 nm emission line. This effect is particularly evident in emission post-extinguishment. Color purity of the post-combustion plasma light emission is found to vary more than either of the other two conditions, which may be due to the low intensity of post-combustion emission, and amplification of noise during calculation of the dominant color (spectrometer integration time during experiments was optimized for sampling during the combustion period rather than the post-combustion period). The chromaticity analysis of the Mg/$NaNO_3$/epoxy formulation suggests overall that emission color of the pyrotechnic produced from microwave enhancement is similar to that of the baseline pyrotechnic emission. The potassium and cesium-based systems were not analyzed because their primary emission bands are outside the visible spectrum.

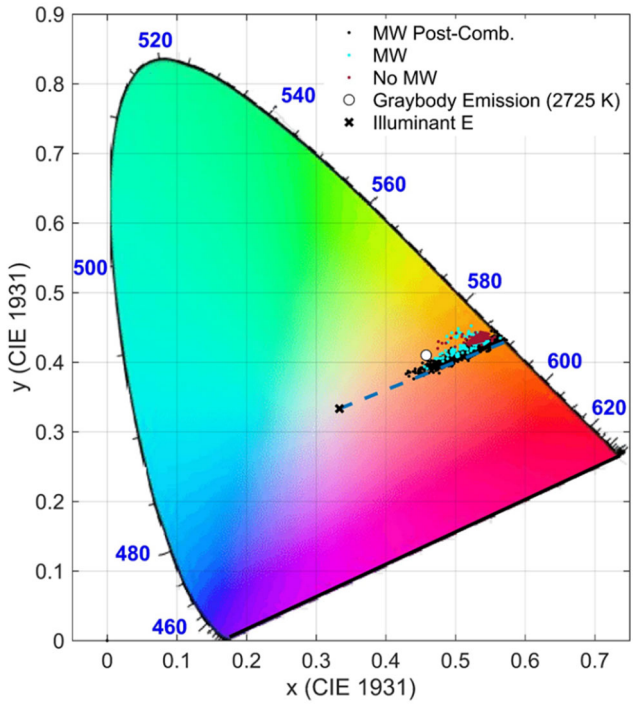

Figure 4. CIE 1931 chromaticity diagram showing time-resolved color and purity of emission from Mg/$NaNO_3$/epoxy pyrotechnics (1) without microwave illumination, (2) with microwave illumination, and (3) emission acquired from microwave illumination of combustion products post-extinguishment. Graybody emission at 2725 K and the Illuminant E point is indicated on the diagram. The dash line represents dominant wavelength of 589.2 nm of varying color purity.

IR Emission Enhancement Measures of time-averaged IR spectral irradiance of each alkali-nitrate formulation (Fig. 5) showed that emission enhancement resulting from microwave illumination of the three formulations extended beyond the visible spectrum and into the IR. Specifically, enhancement of emission from Na I (0.947 μm), K I (1.048, 1.177, and 1.415 μm), and Cs I (1.358, 1.469, 3.010, 3.490, and 3.614 μm) electronic transitions were observed. Additionally, slight emission enhancement of the CO_2 (~4.2 to 4.8 μm) and H_2O (~2.5 to 3.0 μm) IR emission bands were observed for all formulations.

Similar to the visible enhancement results (Fig. 5), little gray body continuum emission enhancement was observed in the near infrared as a result of microwave illumination. This is in contrast to the high concentration of equilibrium-predicted condensed-phase products within the flame (Table 1, 31.2 to 35.2 mol.%) and the high equilibrium flame temperatures of compositions (2943 to 3088 K). In similar studies involving microwave illumination of aluminized AP composite propellants containing $NaNO_3$ dopant [7], continuum emission enhancement of alumina products from aluminum agglomerate diffusion flames was observed as a result of the exponentially temperature-dependent increase in aluminum oxide microwave absorptivity (i.e. microwave loss tangent) that has been observed by others [8]. The high temperature increase in microwave absorptivity, referred to as 'thermal runaway' in microwave sintering literature, is

observed in many ceramics as a result of a shift in heating mechanism from dielectric at low temperatures to eddy current heating at high temperature due to increased charge mobility at higher temperatures [9]. In the aforementioned propellant study, aluminum oxide exists in liquid phase, where its acts as an ionic conductor due to enhanced charge mobility [10]. Consequently, application of an electric field to liquid aluminum oxide can result in more efficient energy absorption and conversion to heat. Conversely for the MgO products within pyrotechnic flames of this study, the MgO remains in solid phase due adiabatic flame temperatures that are lower than the melting point of MgO. Dielectric absorption of solid MgO products may be inefficient at pyrotechnic flame temperatures, as little continuum emission enhancement is observed.

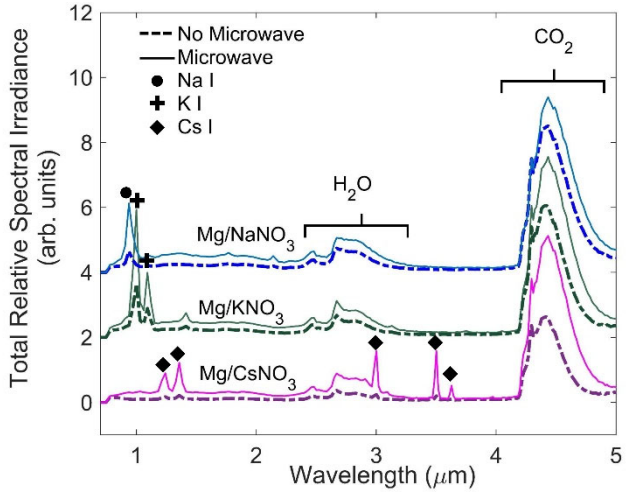

Figure 5. Time-integrated, infrared total spectral irradiance of each Mg/alkali nitrate/epoxy pyrotechnic with and without microwave illumination. Species of significant electronic atomic and molecular emission enhancements observed are noted. Irradiance values for each formulation are offset for presentation purposes.

MW Emission Color Shifting in Mg/PTFE Pyrotechnics

Contrary to pyrotechnics containing alkali earth metals, where luminosity enhancement without chromaticity change has been observed, microwave illumination of pyrotechnics devoid of alkali earth metals can produce distinctly different light emission changes due to interaction with different flame species intermediates and through energy coupling by other means. The effects of microwave illumination on flame structure of a Mg/PTFE pyrotechnic are apparent in the high-speed color images presented in Fig. 6., in which all images have the same exposure. Flame emission without microwave illumination (lower row) is dominated by white to red emission consistent with gray body continuum emission. Microwave illumination results in a visible white and red center (primary) flame core and a blue luminous secondary (sheath) flame region. Emission enhancement in the primary premixed flame is expected to be from condensed phase graphite species ($\varepsilon = 0.7$ to 0.8), which absorb microwave energy dielectrically and optically emit continuum radiation (Fig. 7). The blue light emission enhancement in the secondary flame region is expected to primarily be a result of electronic absorption from the MgO green band (476-521 nm) and the high-intensity MgF/MgO UVA bands (350-390 nm) (Fig. 7a). Finally, the time-

and wavelength-integration of the UV/VIS/NIR Mg/PTFE flame emission during combustion (260 nm to 900 nm) shows that microwave illumination results in an increase in total emission output of 90% (Fig. 7b).

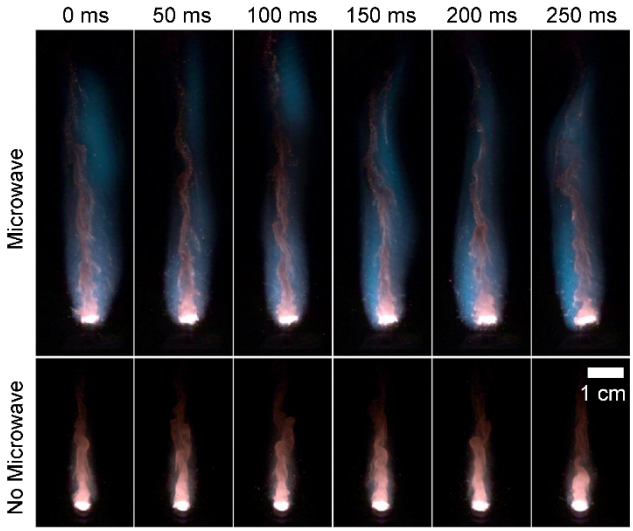

Figure 6. Color image sequences of Mg/PTFE combustion taken with (top) and without (bottom) microwave illumination. Both image sequences have the same camera settings (200 Hz, 4 µs).

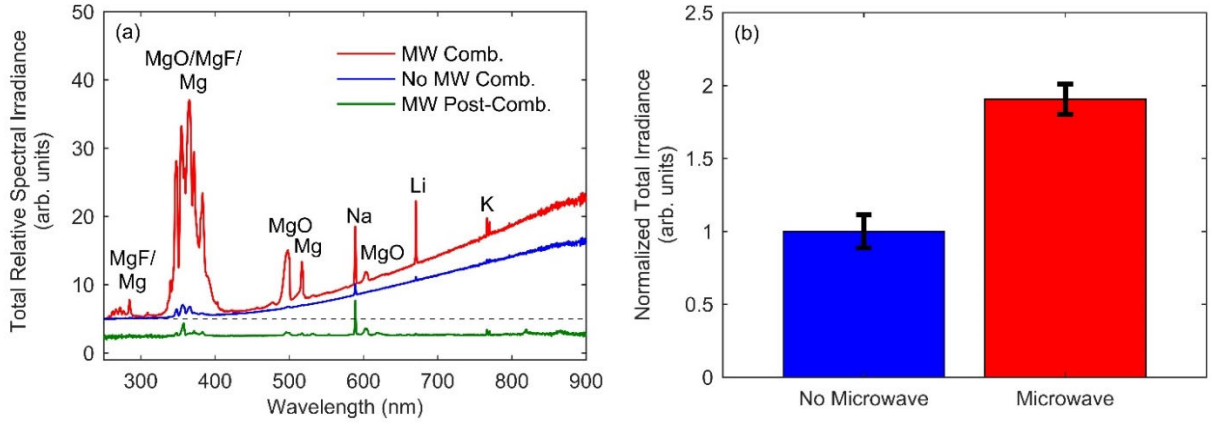

Figure 7. (a) Time-integrated UV/VIS/NIR emission spectra from Mg/PTFE combustion with and without microwave illumination (averages of three tests). Also shown is the post-combustion emission from the pyrotechnic (time-integrated from one trial). Spectra are offset for presentation. (b) Normalized time-integrated and wavelength-integrated total UV/VIS/NIR irradiance (260 nm to 900 nm) of Mg/PTFE emission with and without microwave illumination. Reported values and error bars represent the averages and standard deviations of three experimental trials each.

Materials and Methods

Equilibrium Calculations

Chemical equilibrium calculations were conducted to identify ion and electron populations, adiabatic flame temperatures, and condensed-phase flame products in each formulation. The NASA Chemical Equilibrium with Applications (CEA) code [11] was used to make thermochemical predictions at sea-level atmospheric conditions (1 atm, 10 wt.% excess air). In these calculations, the assumed heat of formation of the epoxy binder (Epon/Versamid; $H_{98}C_{83}O_{14}N_4$) was -3,666 kJ-mol^{-1}. All calculations were conducted with ion chemistry enabled.

Pyrotechnic Formulation and Manufacture

The pyrotechnic formulations used in this study consisted of a magnesium fuel (Firefox; 190-325 mesh) a polytetrafluoroethylene (Sigma Aldrich, 35 micrometer), an alkali nitrate oxidizer, and the aforementioned epoxy binder. Alkali nitrate oxidizers used in formulations consisted of one of the following: sodium nitrate (Hummel Croton Inc., MIL-S-322C, Grade B), potassium nitrate (Hummel Croton Inc., MIL-P-156B, cesium nitrate (American Elements Engineering), strontium nitrate (Pyro Chemical Source), and barium nitrate (Pyro Chemical Source). The epoxy binder used was a two-part thermoset-epoxy consisting of 70 wt. % Epon-813 and 30 wt.% Versamid-140. In most cases, formulations were chosen to maximize adiabatic flame temperature. A listing of all of the formulations investigated in this study is shown in Table 1.

Table 1. Formulations experimentally investigated.

Formulation #	Mg	PTFE	$BaNO_3$	$CsNO_3$	KNO_3	$NaNO_3$	Epoxy
1	28.5	---	---	66.5	---	---	5
2	42.8	---	---	---	52.2	---	5
3	45.6	---	---	---	---	49.4	5
4	50	50	---	---	---	---	---
5	49.95	49.95	---	---	---	0.1	---
6	49.75	49.75	---	---	---	0.5	---
7	47.5	47.5	---	---	---	5	---
8	35	65	---	---	---	---	---
9	65	35	---	---	---	---	---
10	47.5	47.5	5	---	---	---	---

All pyrotechnic compositions were hand-mixed in a grounded pan using a metal spatula in quantities of 10 g or less. First, the fuel and binder were hand-mixed until homogeneous. Oxidizer

was then blended into the fuel/binder pre-mixture. The composition was again hand-mixed until homogeneous. To achieve the desired consolidation density, reactive compositions were shim-pressed in a 6 mm diameter circular die to a nominal length of 9 mm using a Carver 12-ton press and a dwell time of approximately 10 seconds. Prior to combustion, pellets were inhibited with an acrylic lacquer to prevent flame spread down the sides of the pellet.

Boron Propellant Formulation and Manufacture

All propellants were made using a 2:1 bimodal blend of ammonium perchlorate (AP) using 200:90 μm and a hydroxl-terminated polybutadine binder (HTPB). As boron carbide is often sintered using microwave heating, both boron (1 μm, Sigma Aldrich) and boron carbide (10 μm, Sigma Aldrich) additives were used to evaluate the microwave absorption of boron during propellant combustion. The effects of additive loading were investigated by adding 10, 20, or 30 wt% of metal to the propellant. Table 2 shows the exact composition of each propellant used in the study along with their equilibrium performance and theoretical mass density (TMD). Propellants were mixed using a dual-planetary mixer and packed into polyethelyne cylindrical molds to cure for at least 72 hrs. Densities were determined using an analytical balance and caliper.

Table 2. Fuel-rich boron propellant formulations and corresponding equilibrium performance.

	Formulation (wt. %)							
Formulation Name	**Boron**	**Boron Carbide**	**AP**	**HTPB**	**T_{flame} (K)**	**Oxygen Balance**	**TMD (g/cm^3)**	**%TMD**
B10	10%	-	65%	25%	1970	-81.4%	1.540	94.12%
B20	20%	-	55%	25%	1780	-107.0%	1.561	94.60%
B30	30%	-	45%	25%	1750	-132.6%	1.583	94.57%
BC10	-	10%	65%	25%	1850	-82.4%	1.545	95.08%
BC20	-	20%	55%	25%	1760	-108.9%	1.574	96.29%
BC30	-	30%	45%	25%	1740	-135.5%	1.602	94.24%

Microwave Combustion Cavities

Free-Space Microwave Cavity

In order to observe the interaction of electromagnetic fields with pyrotechnic flames in a stand-off environment similar to application, an instrumented, free-space microwave combustion cavity was developed. The cavity, a 6 m wide by 3 m tall by 1.5 m wide sealed steel enclosure was modified with faraday cage air inflow and outflow on the top and bottom of the cavity and a microwave safe door and observation window on the side for the cavity for physical and optical access, respectively. The back side of the cavity is lined with microwave absorptive ceramic tiles enabling simulation of a free-space field environment. A photo and diagram of this experiment are shown in Fig. 8. The cavity consists of a 2 kW magnetron, circulator and dummy load for magnetron protection, diodes for forward and reflected power measurement, and a selectable high-

power antenna for field focusing. Additional equipment used for measurement and calibration include power meters, attenuators, oscilloscopes, and a power delivery circuit.

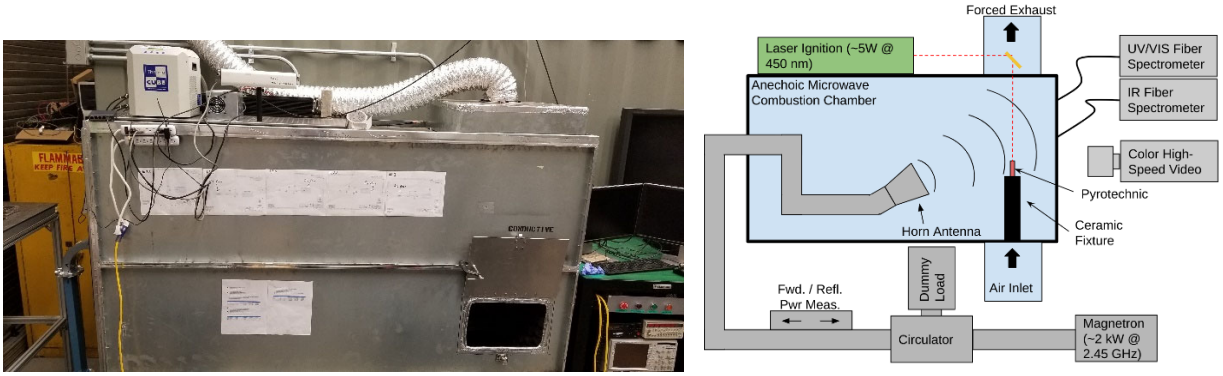

Figure 8. Left: Photo of free-space microwave combustion cavity. Right: Diagram of free-space combustion cavity. Diagnostics observe the combustion plume from the sized through access door through a faraday cage (not shown).

In order to ensure the microwave cavity replicates a free-space environment and to determine the field strength distribution within the cavity resulting from different antenna conditions, the field strength distribution within a cavity containing perfectly absorbing walls was simulated and compared to experimental measurements of field strength made within the cavity. Utilizing COMSOL Multiphysics, the distribution of the field in the free space cavity was modeled. Briefly, three different antennas conditions were modeled, (1) no horn (WR-284 waveguide), (2) with a 10 dBi gain horn (Pasternack, PW9863-10), and (3) with a 20 dBi gain horn (Pasternack, PW9863-20). The field strength distribution within the cavity is shown in Fig. 9 and field strength as a function of the antenna exit plane using different antennas is shown. This data is compared with measurements of power losses (S_{21}) at varying stand-off distance within the cavity (Fig. 10) in order to validate the free space condition of the cavity. In order to perform power loss measurements, a calibration was performed of the entire system using a power meter (HP 437B) and signal generator (Stanford Research Systems SG384). After the power losses of the waveguide power delivery circuit was calculated, a receiving antenna was placed at varying distances from the open waveguide port, and power was measured and power loss calculated.

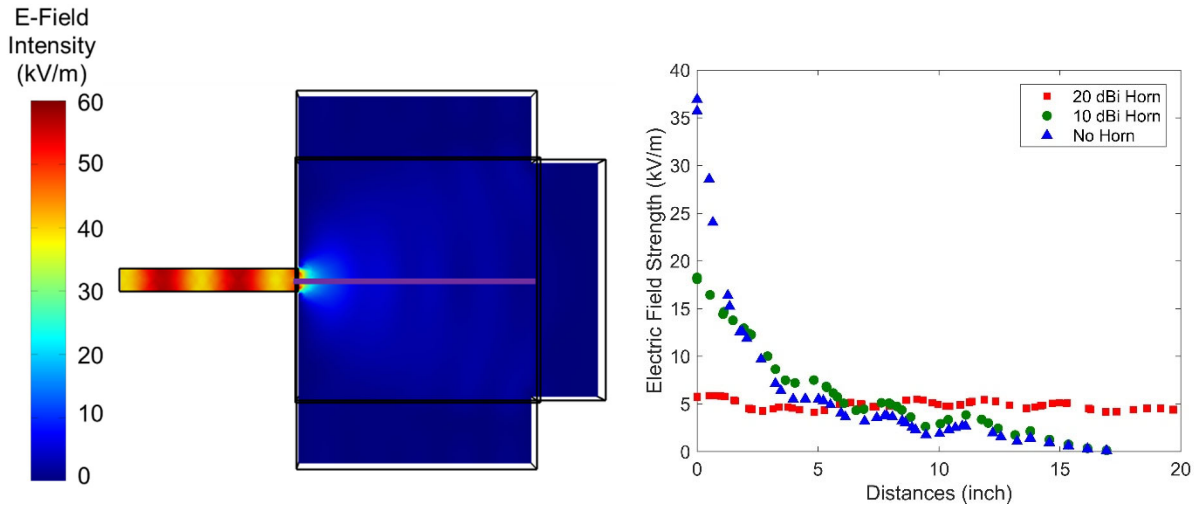

Figure 9. Left: COMSOL simulation of E-field distribution within the free-space cavity using an open waveguide (no antenna) condition. Simulated electric field strength as a function of distance along the centerline of the cavity. The output power of the antenna port was set to 2 kW.

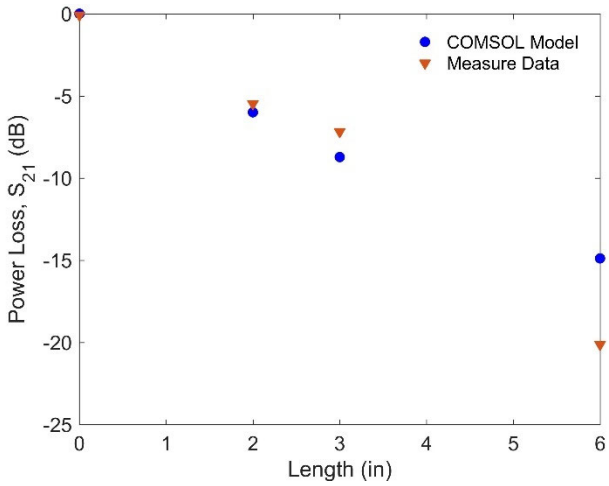

Figure 10. Power loss (S_{21}) as a function of distance away from an open waveguide port (WR-284) in the free space cavity. COMSOL Multiphysics was utilized to compared measured values, in which an average power loss was calculated by matching the receiving antenna cross-sectional area.

Multi-Mode Cavity

A multimode microwave cavity (Fig. 11a) connected to an 870 W, ~2.46 GHz magnetron and a high-voltage power supply modulated at 60 Hz (50 % duty cycle) was used for experiments. The pyrotechnic was placed in an electric-field (E-field) antinode atop a microwave-transparent polytetrafluoroethylene (PTFE) block. The location of the field antinode was verified both experimentally and by numerical simulation. Experimentally, the E-field antinode location was found by imaging a liquid crystal film placed at various locations within the unloaded cavity during microwave application. The E-field distribution within the cavity was also determined by modeling the cavity using COMSOL Multiphysics 5.1 (Fig. 11b). The E-field strength in the volume

occupied by the pyrotechnic flame was estimated via dielectric heating of a 100 cm^3 volume of water according to the National Bureau of Standards procedure [12], yielding an average electric field strength of 2.1 ± 0.1 kV/m within the antinode of interest. Pyrotechnic samples were microwave-ignited using an electromagnetically absorbing thin film (polyester/vapor deposited aluminum film), which was placed on the top of pyrotechnics and heated until ignition. For baseline experiments (without microwave), the pyrotechnic composition was ignited directly using a hot wire ignition source. Energetic material articles were ignited using a 450 nm, 5W, CW laser through a small hole located above the sample.

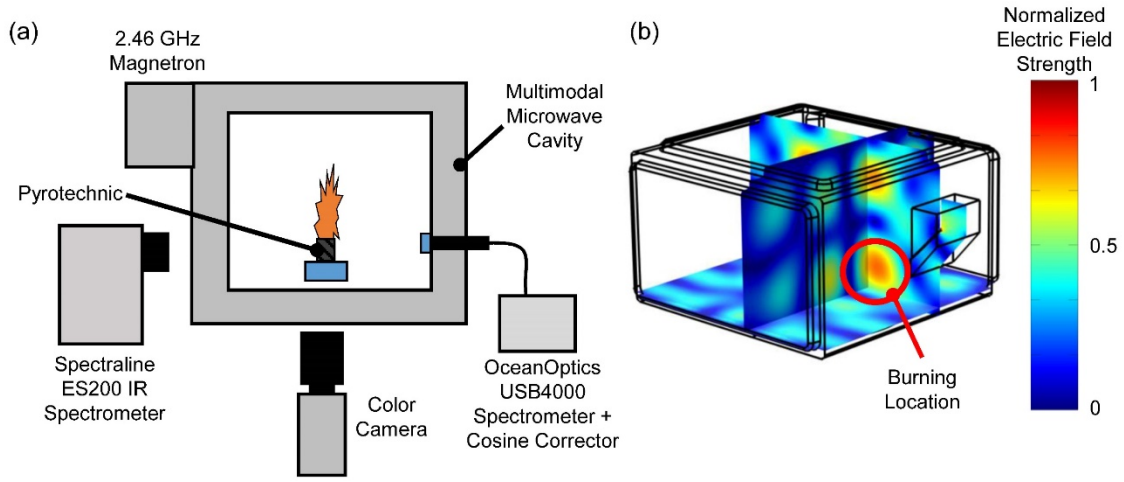

Figure 11. (a) Schematic of the experimental setup of the microwave cavity. Experiments were monitored with a color high-speed camera and two spectrometers (VIS/NIR and IR). (b) Distribution of the mean electric field strength simulated using COMSOL within the microwave chamber. The red circle indicates the location of the pyrotechnic flame, which is located at an E-field antinode with an average field strength of 2.1 ± 0.1 kV/m in a 100 cm^3 volume of water.

Premixed, Seeded Burner

Burner Design and Manufacture

A burner was designed to allow solid particles to be injected axially through an annular, premixed flame. Premixed gas can be fed through one port or each gas can be injected individually through 2 ports and mixed inside the burner. The current configuration uses a T-connection on a single port to combine the oxidizer and fuel gas prior to entering the burner chamber. A flame arrester connection (McMaster-Carr) is attached to each gas line to prevent flashback at the mixing location. The gas is then fed into the base of the burner (Fig. 12c) which contains a removable tube that allows the injected particles to flow through the gas chamber to the burner outlet. The gas chamber of the burner is attached to the base using six bolts and sealed using an o-ring(McMaster). The gas flows into the base and up into the annular gas chamber (Fig. 12b) which is filled with glass beads to promote gas mixing and reduce explosive volume in the event of a flashback. The chamber tapers down to the outlet shown at the top of the center part and flows out of the cutout in the top of the burner (Fig. 12a). The top of the burner is threaded and mates with the threads of the chamber to allow for a metal mesh to be held in place between both parts. This offers additional

flashback prevention at the outlet of the burner while still allowing a hole to be cut in the mesh for the particles to exit the tube in the center of the burner.

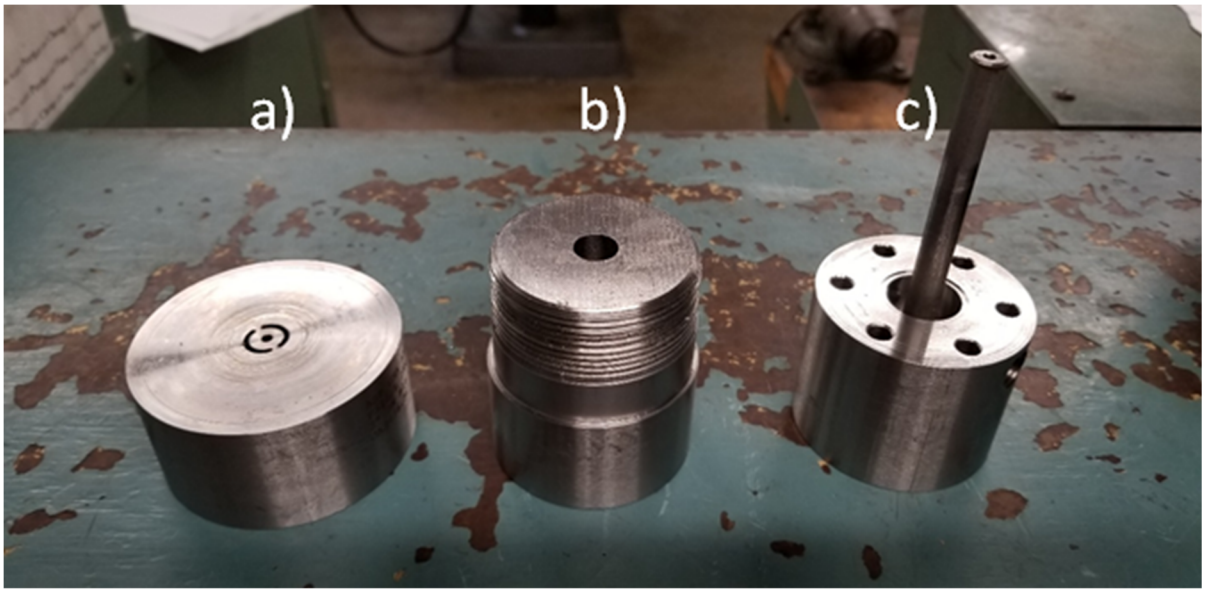

Figure 12. Disassembled premixed gas-phase burner including the top "cap" of the burner (a) the gas mixing chamber section (b) with external threads to mate with the top and the base with the particle feeding tube (c) attached, where the premixed gases enter laterally into the burner.

Particle and Aerosol Feeder Systems. Two different feeder systems were designed and manufactured to allow both solid particles and aerosolized alkali metals to be injected into the burner flame. Solid particles are first brushed onto a large diameter screw (3/4") which is inserted into a brass tube sized so that the inner diameter of the tube is the same as the outer edge of the screw threads. A hole is then drilled through the edge of the tube so that a small diameter tube (1/16" OD) could be inserted into the large diameter tube. This small tube was filed down on one edge into a triangular shape that mates with the threads of the feeder screw. Inert gas (nitrogen) then flows through the tube to blow the solid particles off the screw and into another, slightly larger tube (1/4" OD) and into the burner. The light coating of particles placed on the screw allows for a very small number of particles to be entrained into the flow, allowing observation and analysis of individual particles or very small clusters of particles.

A feeder system was also developed for injecting aerosolized alkali metals into the burner and is based upon a TSI 3076 spray atomizer. The spray atomizer was not able to be tested during this funding cycle due to delays in obtaining the spray atomizer, which was in high demand for use in COVID-19 droplet transport studies. Water solutions of alkali metal nitrates are injected using the aerosolizer and flexible Nylon tubing attached to a pipe fitting at the base of the burner. A water solution of NaCl and $CaCO_3$ or $Ca(HCO_3)_2$ was placed in the aerosolizer. The calcium carbonate or bicarbonate is added to determine the amount of Ca in the particle flow through the burner flame, which corresponds directly to the amount of sodium present in the flow CITE. This mixture is used to calibrate the flow rate of carrier gas for the desired quantitative flow rate of alkali metal.

Flame Temperature Measurement. Spatial temperature measurements of the burner flame are accomplished using 2-color pyrometry. A thin alumina rod (1/16" diameter) is suspended vertically above the burner along the axis of the burner flame, coincident with the path of the particles through the central feeder tube. The burner is ignited, and the rod is allowed to reach a steady-state condition within the flame. The rod is thin enough to avoid appreciable temperature variation in the radial direction (Biot number < 0.01) and the end of the rod is placed at the top of the burner. Filtered light at 800 and 905 nm (10 nm FWHM) is collected using a high-speed camera (Phantom ir300) with a K2 magnifying lens (Infinity Optics). The imaging system was calibrated by imaging a hole within a ceramic brick (approximate blackbody) placed inside a tube furnace.

Point measurements of flame temperature were also determined by using a vertically-actuating, fiber-coupled spectrometer. A UV-VIS spectrometer (USB4000, OceanOptics, 25 μm slit, 600 lines/mm, ~100Hz, 10 ms integration time) was coupled with a 1 mm, multimode fiber and attached to a linear actuator with an achromatic lens and focusing optic to image a ~1 mm section of the alumina rod. By sweeping the fiber vertically along the rod and taking periodic spectra, an estimate of the condensed-phase temperature profile of the rod can be determined by graybody fitting (procedure discussed in later sections)

Combustion Diagnostics

A Phantom v7.0 color complementary metal-oxide semiconductor (CMOS) camera and Canon zoom lens were used to capture high-speed video of the pyrotechnic combustion (500 Hz, 10 to 100 μs exposure, Figs. 8,9). To monitor the VIS/NIR spectral emission, an Ocean Optics USB4000 spectrometer (200 to 900 nm, 25 μm slit, 600 lines/mm, ~100Hz, 10 ms integration time) was used with an OceanOptics multimode fiber (400 μm diameter, P400-0.25-SR). Light was collected onto the fiber end using a cosine corrector (OceanOptics, CC-3-UV-S) to capture a large field of view within the white (optically reflective) microwave cavity. Prior to testing, the VIS/NIR spectrometer was calibrated using a deuterium tungsten-halogen light source (OceanOptics, DH-2000-CAL) to correct for detector responsivity and achieve relative spectral irradiance measurements. Acquisition of spectra of molecular emission used for temperature fitting were collected by a high resolution, 0.5 m long Andor spectrometer with Andor iDus detector.

Experimental Data Post-Processing

Time-Integrated, Total Emission, Chromaticity, and Luminosity

Emission spectra were post-processed using MATLAB to correct for dark noise level and detector responsivity. From calibrated spectra, measures of time-integrated spectral emission were calculated as

$$E_{e,total}(\lambda) = \frac{1}{m_{sample}F_s}\sum_{i=1}^{n} E_e(\lambda, t_i), \quad (1)$$

where $E_{e,total}(\lambda)$ is the time-integrated relative spectral irradiance per gram pyrotechnic for the entire burn (arb. units per gram), m_{sample} is the pyrotechnic article mass, F_s is the spectrometer sampling frequency, $E_e(\lambda, t_i)$ is the relative spectral irradiance, λ is wavelength, and t_i is experimental time. A measure of time-integrated emission is calculated by numerically integrating $E_{e,total}(\lambda)$ over all wavelengths between 400 to 880 nm. Emission outside of this spectral range suffered low signal to noise levels and was omitted from the analysis.

The dominant visible wavelengths from the pyrotechnic flame emission were calculated for comparison on a CIE 1931 chromaticity diagram. In doing so, the procedure of Ref. [13] was followed. Briefly, tristimulus values for each spectrum in the time series,

$$X_i(t_i) = \int_{\lambda=0}^{\infty} E_e(\lambda, t_i)\bar{x}(\lambda)d\lambda \qquad Y_i(t_i) = \int_{\lambda=0}^{\infty} E_e(\lambda, t_i)\bar{y}(\lambda)d\lambda \qquad Z_i(t_i) = \int_{\lambda=0}^{\infty} E_e(\lambda, t_i)\bar{z}(\lambda)d\lambda \quad (2)$$

were calculated, where $X_i(t_i), Y_i(t_i)$, and $Z_i(t_i)$ are the tristimulus values of the relative spectral irradiances in the time series, and $\bar{x}(\lambda), \bar{y}(\lambda)$, and $\bar{z}(\lambda)$ are the CIE 1931 two-degree field of view color-matching functions. The chromaticity coordinates, $x_i(t_i)$ and $y_i(t_i)$ of each spectrum in the time series are then calculated as

$$x_i(t_i) = \frac{X_i(t_i)}{X_i(t_i)+Y_i(t_i)+Z_i(t_i)} \qquad y_i(t_i) = \frac{Y_i(t_i)}{X_i(t_i)+Y_i(t_i)+Z_i(t_i)}\,. \quad (3)$$

To capture the infrared emission spectra, a Spectraline ES200 IR spectrometer (1.2 to 5.5 μm, 1,320 Hz, ~0.03 μm resolution) was used. The collection angle of the spectrometer is 0.5 degrees and captured an approximately 0.5 mm wide by 6 mm tall area at the experimental distance. This sampling volume was positioned 25 mm above the pyrotechnic sample. As such, unlike visible spectra, which are representative of entire flame emission, IR emission spectra are from a small volume above the pyrotechnic article and not representative of the entire flame. Prior to use, the IR spectrometer was calibrated using a gray body source placed at the experimental observation distance to produce measures of absolute irradiance. IR emission was post-processed in MATLAB to calculate time-integrated emission. The rise time of the E-field is expected to be short (on the order of milliseconds or less), which is much shorter than UV/VIS instrumentation that is used to assess the degree of light emission enhancement.

Continuum Temperature Calculation

Temperature is determined by fitting the collected spectra to Planck's equation as a function of varying emissivity and temperature. As shown in the in-house fitting tool below (Fig. 13), only spectral regions without molecular or atomic emission features and with high signal to noise are used for the fitting and only the middle 90% of the burning time is used for the analysis to avoid use of temperatures from transient ignition and extinguishment phases.

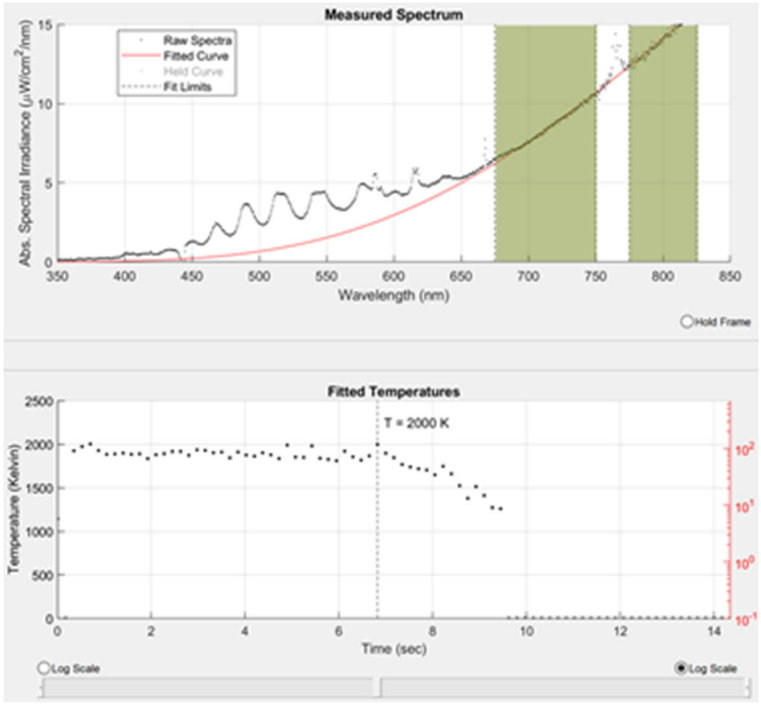

Figure 13. An example of the MATLAB GUI used to evaluate the condensed-phase combustion temperature by fitting of continuum emission regions (650 – 750 and 775-825 nm shown) to a graybody curve.

Computational Methods

Computational analysis of microwave-enhanced pyrotechnic emission was conducted mainly by analyzing the short-timescale processes (<50 ns) thought to directly govern VIS/NIR emission by atomic species. These included: (1) the penetration characteristics of applied microwave fields into high-temperature weakly-ionized pyrotechnic plumes, (2) the energy transfer to free electrons resulting in non-equilibrium electron energies, (3) the augmented emitter population obtained by electron-neutral excitation collisions, and (4) the radiation transfer associated with enhanced emission. These areas were initially linked by development of a simplified quasi-steady state 1D model and are being incorporated into more complex models capable of predicting the observed spectra and the long-timescale coupling of microwaves with conventional chemical kinetics and fluid dynamics. A diagram describing the numerical code development, including completed tasks and future tasks is shown in Fig. 14.

As model development progressed, three major obstacles were encountered, which were overcome. Firstly, a fundamental trade-off was identified between the density of alkali species and microwave penetration. While larger alkali densities improved the quantity of potential emitters and free electrons available for energy transfer, the high density of ions could heavily dampen or altogether reflect incoming microwaves. This trade-off shaped subsequent analysis, and suggested emission enhancement could be improved by pursuing lower equilibrium alkali densities, lower temperatures, and microwave sources with higher frequencies.

Secondly, significant limitations were discovered in the tools available for solving the electron Boltzmann equation in the presence of alternating fields. Early research identified that the widely-available BOLSIG+ code could not accurately simulate electrons enhanced by microwaves in atmospheric-pressure conditions with molecular gases. This shortfall is due to the assumption of field frequencies being either sufficiently high or low to prevent individual regions of the electron energy distribution (EEDF) from oscillating in phase-with the alternating field. The high-pressures and exceptionally efficient electron energy transfer to vibrational nitrogen at 1-5 eV posed this exact problem, doubly so because electron-alkali collisions that generate alkali emitters also reside in the 1-5 eV range. This issue prompted further Monte Carlo analysis and identified the need for improved Boltzmann techniques in future research.

Lastly, the simulation of VIS/NIR spectra for alkali pyrotechnics was hampered by the complex phenomenon associated with the resonant alkali line shape broadening, which was not trivial to incorporate into radiation transfer simulations. At high pressures, the thermodynamic favorability of alkali-alkali quasi-molecules leads to long-duration perturbation of emitter energy states, resulting in extreme line broadening that can generate spectral features at or above 200 nm from line center. Incorporating quasi-static theory greatly improved agreement between simulated and experimental spectra.

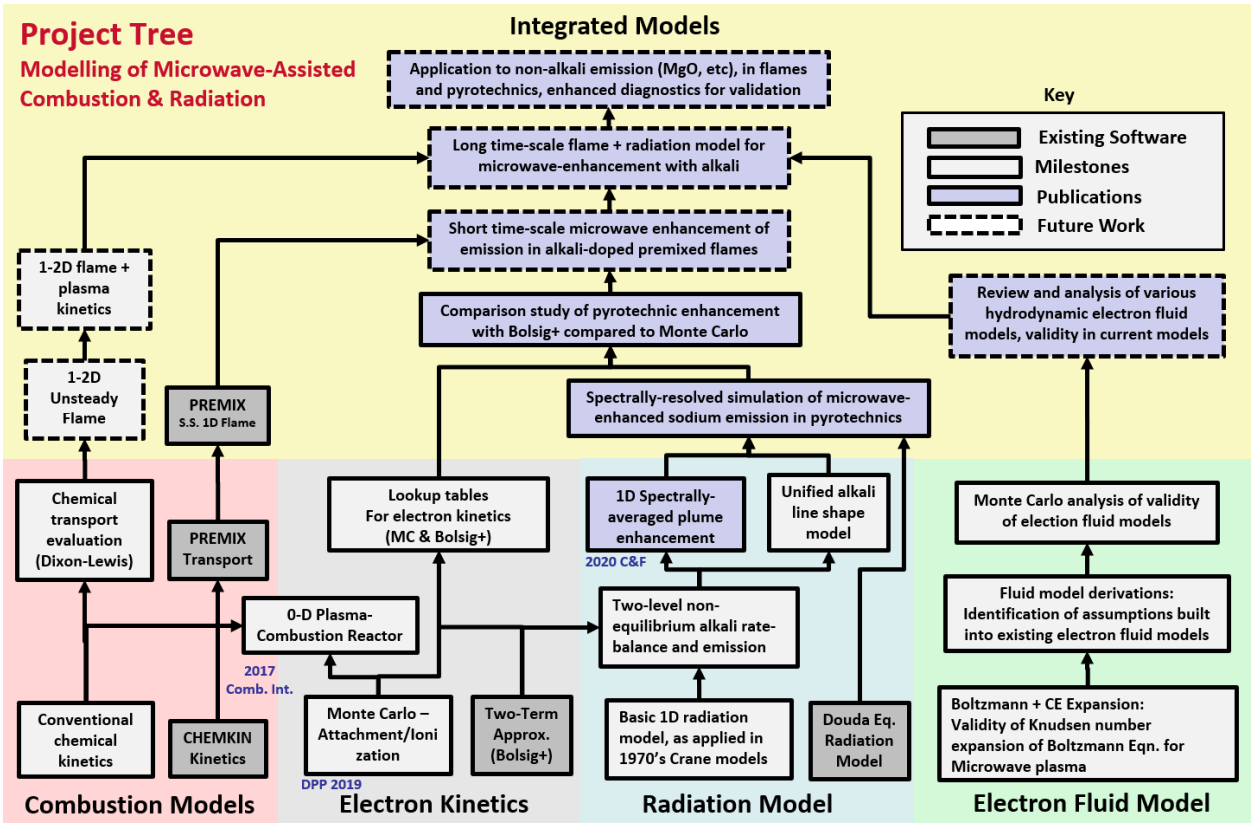

Figure 14. Project tree for modeling microwave-enhanced combustion and emission, relevant for pyrotechnic plumes and seeded flames. Milestones broken down into combustion models, electron kinetics, electron fluid models, and radiation-transfer models, which synthesis in integrated models is being developed.

1. Microwave-Enhanced (VIS/NIR) Alkali Emission Model

Comprehensive modeling of microwave-enhanced pyrotechnics is a formidable challenge. A high-fidelity approach would require coupling radiation-transfer, electric field propagation, chemically reacting fluid dynamics, and non-equilibrium electron kinetics, covering a vast range of timescales over multiple dimensions. As a first step, we introduce a collisional-radiative model with the minimum components needed to capture the proposed WMIP effect for atomic alkali emission in quasi-steady state over plasma and optical timescales ($\approx 0.5 - 50\ ns$). This requires solving a radiation transfer equation where both the emission rate and probability of radiation escape vary as a function of distance into a model plume. The emission coefficient varies according to a kinetic rate balance regulated by the local electric field strength, which in turn is determined from the penetration characteristics of an applied microwave field. The result is a spectrally-integrated solution for radiance emitted perpendicular to the plume surface. Ratios of radiance with and without applied fields are then directly compared to ratios of irradiance in experiments computed in Eqn. 1.

Four key assumptions were necessary to simplify the dimensions and number of required parameters. They are: (1) Except for alkali species, the plume is treated as a homogenous and quiescent post-combustion zone with a prescribed temperature and alkali mole fraction deviating from CEA equilibrium, with a hard interface to the ambient environment; (2) the microwave field does not significantly perturb the plume from Saha equilibrium or increase the plume temperature; (3) Planck equilibrium is maintained within the plume such that only a minor fraction of radiation escapes and is ultimately detected; and (4) the rates of alkali absorption and emission are negligible compared to kinetic pathways. As heat and mass transfer from entrained air are expected, the plume temperature T_0 and alkali mole fraction X_{alk} are left as parameters to represent the conditions for the outer layer of the plume, averaged over time and plume surface.

For a single atomic alkali transition or doublet, the resulting radiance is a convolution integral of the rate of radiant energy emission and the frequency-integrated probability of photon escape from the plume. Integrating from the plume center line (s=L) to the edge (s=0), this takes the base form,

$$I = \int_0^L \epsilon(s)\mathcal{T}(s)ds \qquad (4)$$

where: s is the normalized plume depth described graphically in Fig. 15, I is the radiance ($Wm^{-2}sr^{-1}$) at the surface of the plume; $\epsilon(s)$ is the volumetric emission coefficient ($Wm^{-3}sr^{-1}$) at a given depth; L is the width of the plume slab; and $\mathcal{T}(s)$ is the transmittance, or normalized probability of photon escape to $s = 0$. A sample configuration is shown in Fig. 15, where the field strength, transmittance, and emission coefficient all decline until a critical depth $s = \delta$, or skin depth, where the field effect becomes negligible.

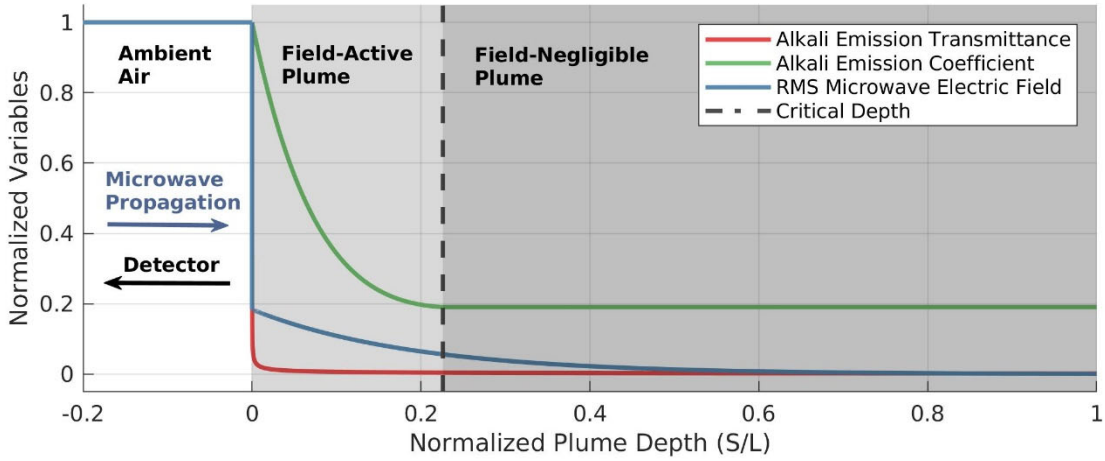

Figure 15. Example configuration of the homogenous plume model with an incident electric field propagating left to right, perpendicular to the plume surface. Radiance is computed at surface, $s = 0$, simulating light available for detection.

The derivation of transmittance relies on the presence of resonant line broadening reviewed by de Groot and Vliet [14], and the frequency-averaged escape factors reviewed by Drawin and Emard [15]. The result depends only on the depth, s, and the wavelength λ.

$$\mathcal{T}(s) = s^{-\frac{1}{2}}\sqrt{\frac{\lambda}{4\pi^2}}\,, \quad s > \frac{\lambda}{4\pi} \tag{5}$$

For Eqn. 4, the integration of $s < \lambda/4\pi$ can be neglected, as $L \gg \lambda$. The emission coefficient is obtained by

$$\epsilon(s) = A_{21}\frac{h\nu}{4\pi}N_2 = \frac{1}{\lambda^3}\left(\frac{g_1}{g_2}\frac{2\pi e^2}{\epsilon_0 m_e}f_{12}\right)\frac{h}{4\pi}N_2 \tag{6}$$

where A_{21} is the coefficient for spontaneous emission, g_1/g_2 is the ratio of ground to excited state degeneracies, ν is the photon frequency, f_{12} is the oscillator potential, and N_2 is the non-equilibrium excited-state alkali population. The emission coefficient for sodium and potassium doublets were computed as single transitions. For cesium, only the higher-energy transition, Cs 6P(3/2), was measured and simulated. The local N_2 population is obtained using assumption (4), which neglects emission and absorption in the steady-state rate balance

$$N_2(s) = N_1\frac{K_{M+}X_{mol} + K_{E+}(s)X_e}{K_{M-}X_{mol} + K_{E-}(s)X_e} \tag{7}$$

where N_1 is the ground state alkali density, K_{M+} and K_{M-} are the respective rate coefficients for alkali-neutral excitation and quenching, K_{E+} and K_{E-} are the same but for alkali-electron rates,

X_{mol} is the mole fraction of molecular background gas, and X_e is the mole fraction of free electrons. N_1 is defined through the parameter for alkali mole fraction X_{alk}. The electron mole fraction, X_e, is obtained through Saha equilibrium, and X_{mol} is set by CEA equilibrium calculations shown in Table 1. Out of necessity, the quenching rate of all molecular species is assumed to match that of molecular nitrogen, which is already a sizeable fraction of the mixtures shown in Table 1. Because all the alkali-molecule interactions are treated as alkali-nitrogen, the effect of air entrainment on Eqn. 7 is contained implicitly in the free parameter X_{alk} and its relationship with X_{mol}.

At flame and pyrotechnic temperatures, the quenching rate K_{M-} approaches the thermal limit

$$K_{M-} = \sigma_A \sqrt{\frac{8k_b T_0}{\pi \mu_{eff}}} \tag{8}$$

where σ_A is a cross section specific to each alkali, and μ_{eff} is the effective reduced mass of the alkali species with N_2 [16]. The complementary excitation rate K_{M+} is then constrained by the requirement of detailed balance. Using Maxwell-Boltzmann statistics, an Arrhenius expression for K_{M+} can be obtained

$$K_{M+} = \left[\sigma_A \sqrt{\frac{8k_b}{\pi \mu_{eff}}} \frac{g_2}{g_1}\right] T_0^{\frac{1}{2}} \exp\left(-\frac{hc}{\lambda} \frac{1}{k_b T_0}\right) . \tag{9}$$

The electron-alkali rate coefficients K_{E+} and K_{E-} are determined from the BOLSIG+ code, which uses a two-term approximation to the Boltzmann equation to solve for the non-equilibrium electron energy distribution with an applied field effects [17]. Cross-sections for equilibrium products are obtained from the LXCat database for N_2 [18], CO [19], and Mg [20], which are used to approximate non-alkali combustion products. Alkali cross sections for elastic, excitation, and ionization are obtained for sodium, potassium, and cesium [21–23]. The resulting rates are computed as functions of the reduced root-mean square (RMS) electric field (E/n_0, units of Td) and fitted to quadratic and logarithmic functions of electric field magnitude $E(s)$ once total number density inside the plume n_0 is known.

$$K_{E+} = P_1 E(s)^2 + P_2 E(s) + P_3, \quad K_{E-} = Q_1 + Q_2 \ln(E(s)) \tag{10}$$

The microwave field solution $E(s)$ is computed using Fresnel equations for an electric field in air incident on an absorbing medium:

$$E(s) = E(0)\left[\frac{2}{1+|\widetilde{\mu_0}|}\right]\exp(-s\alpha_0) \tag{11}$$

where $E(0)$ is the incident RMS electric field magnitude, determined from the parameter for applied reduced field (E_{RMS}/n_{amb}) in the cavity outside the plume. The magnitude of the complex index of refraction $|\widetilde{\mu_0}|$ and attenuation coefficient α_0 are calculated for plume conditions using the equations for collisional plasmas listed by Laroussi [24], where electron collision frequency is estimated from BOLSIG+ results.

A complication of using the BOLSIG+ solver is that K_{E+} curve fits are typically invalid below 10 to 20 Td. This occurs when the field strength becomes negligible and thermal electrons become the dominant source of excitation. The reduced field where this transition occurs (defined as $(E/n_0)^*$), can be obtained by inspection of Eqn. 10. The skin depth $s = \delta$ of this transition to a zero-field regime is found by manipulation of Eqn. 11.

$$\delta = -\frac{1}{\alpha_0} ln\left[\frac{(E/n_0)^*}{(E(0)/n_{amb})}\left(\frac{T_{amb}}{T_0}\right)\left(\frac{1+|\widetilde{\mu_0}|}{2}\right)\right] \tag{12}$$

where the minimum skin depth for is $\delta = \lambda/4\pi \approx 0$. Then Eqn. 4 for total radiance can be solved piecemeal with Eqn. 5-12 by isolating the zero-field emission term $\epsilon(\delta)$:

$$I = \int_{\lambda/4\pi}^{\delta} \epsilon(s)\mathcal{T}(s)ds + \epsilon(\delta)\int_{\delta}^{L}\mathcal{T}(s)ds \quad . \tag{13}$$

Finally, the ratio of radiance with and without microwave application can be obtained as

$$R = \frac{\int_{\lambda/4\pi}^{\delta}\epsilon(s)\mathcal{T}(s)ds+\epsilon(\delta)\int_{\delta}^{L}\mathcal{T}(s)ds}{\epsilon(0)\int_{\lambda/4\pi}^{L}\mathcal{T}(s)ds}, \tag{14}$$

where the primary unknown parameters are E_{RMS}/n_{amb}, T_0, and X_{alk}.

2. Electron Kinetics in Microwave Combustion & Boltzmann Equation Solutions

In order to determine whether the limitations of the BOLSIG+ Boltzmann solver were acceptable for simulating electron kinetics in microwave-enhanced plumes, Monte Carlo simulations were employed to predict average energy and collision rates in the relevant gas mixtures and state. This involved simulating individual electron trajectories in an alternating field with energy-dependent collisional rates resulting from the various elastic, vibrational,

electronic, ionization, and attachment processes. Departure from BOLSIG+ was expected for vibrational and electronic excitation frequencies on the order of field frequencies.

Additionally, the effects of non-conservative electron collisions (attachment/ionization) needed careful accounting in simulations. Benchmarks were introduced and tested for results using known attachment cross-sections, with high accuracy and precision achieved for sufficient electron samples. With these results, simulations were conducted in atmospheric flame conditions to identify the degree of possible deviation between the BOLSIG+ code and more capable Monte Carlo techniques.

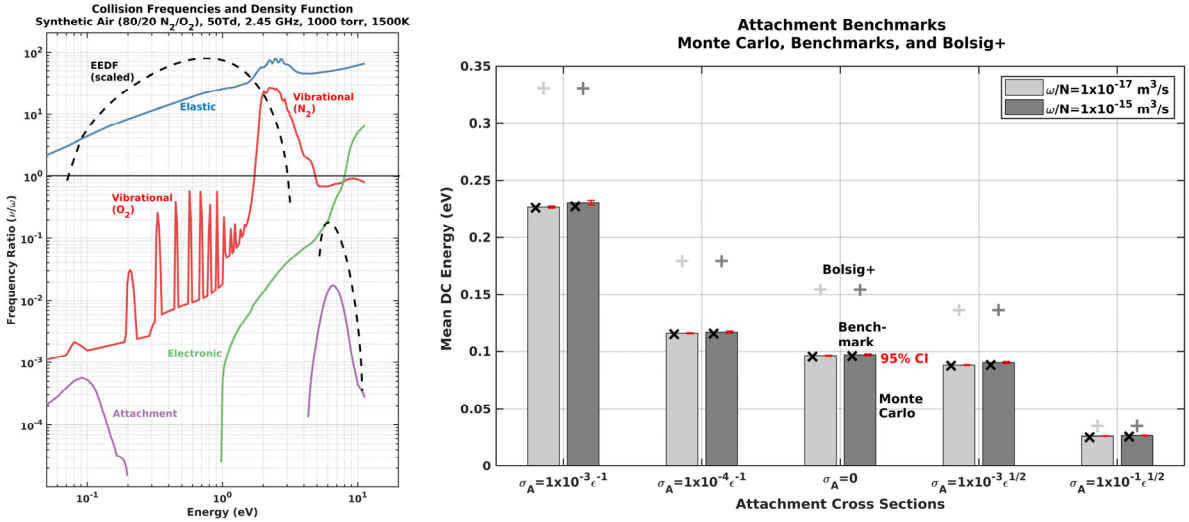

Figure 16. (Left) Electron collision rates in atmospheric gas relative to field frequency (right) Monte Carlo benchmarks for attachment compared to BOLSIG+ simulations

Additionally, the possibility that conventional Boltzmann solvers may be inaccurate for present conditions suggested other models relating to electron kinetics in microwave plasmas may need to be examined. Chiefly, the existing hydrodynamic models for electron motion available in literature (mainly the drift and diffusion equation) also rely on similar assumptions about the EEDF being time-independent. Some preliminary analysis was conducted to assess existing hydrodynamic models and identify possible alternatives, but results are still forthcoming.

3. Non-Equilibrium Microwave-Enhanced Reacting Flow Models

As shown in the project tree, the next step after simulating 1D radiation enhancement over plasma-kinetic timescales is to incorporate the accumulated effects of microwave coupling on timescales relevant to conventional chemical reactions and fluid dynamic processes. This added capability will be crucial for modeling the emission and combustion enhancement in alkali-seeded flames, as well as for improving predictions of free-alkali species in post-combustion pyrotechnic plumes.

However, the time-scale disparity between plasma-kinetic processes and bulk fluid motion pose a considerable challenge, and this model remains in development. Initial progress was made to couple the chemical and plasma kinetic systems in a zero-dimensional reactor, with electron-neutral rates provided by tabulated Monte Carlo or BOLSIG+ solutions. This framework can be deployed once an unsteady chemical-reacting flow solver is developed or adapted for the present systems.

Results and Discussion

Exploration of the Effect of Free Electron Concentration on Field-Flame Coupling in a Free-Space E-Field

Measurements of pyrotechnic light emission enhancement from the multimodal microwave cavity demonstrated the ability to enhance light emission of a Mg/alkali nitrate pyrotechnic and light/color of a Mg/PTFE pyrotechnic. To examine pyrotechnics combustion in an application relevant field condition, a free space cavity was utilized to study various pyrotechnic formulations. This initial work examined Mg/PTFE based pyrotechnics, while exploring the effects of enhancing the free electron population with the addition of an easily ionizing material. NASA CEA simulation of a 0-D combustion equilibrium was utilized to discover 4 different formulations of 1:1 wt. ratio Mg/PTFE, in which free electron populations increase with addition of $NaNO_3$, as seen in Fig 17. The premise for doping in small quantities of alkali into the Mg/PTFE were twofold: (1) to understand how presence of both strongly ionized species (e.g. sodium) and weakly ionized species (e.g. MgO) in the flame affect propensity of the E-field to modulate either a color shift or luminosity amplification, and (2) numerical simulations have suggested that far less alkali may favorably affect field penetration. The rational for selection of low quantities of alkali dopant, though not a direct indication of flame reflectivity, can be simply understood from the results of equilibrium calculations as a function of sodium nitrate alkali additive (Fig. 17). These formulations included 0-5 wt.% addition of $NaNO_3$, where free electron concentration can be enhanced by ~25 times within this range. It should be noted, however, that the free electron concentrations of these alkali-doped Mg/PTFE formulations are still orders magnitude below the free electron concentrations of stoichiometric Mg/alkali nitrate formulations. With higher amount of $NaNO_3$, free electron populations remain constant until ~30% $NaNO_3$ addition, where higher amounts of $NaNO_3$ may lead to shielding.

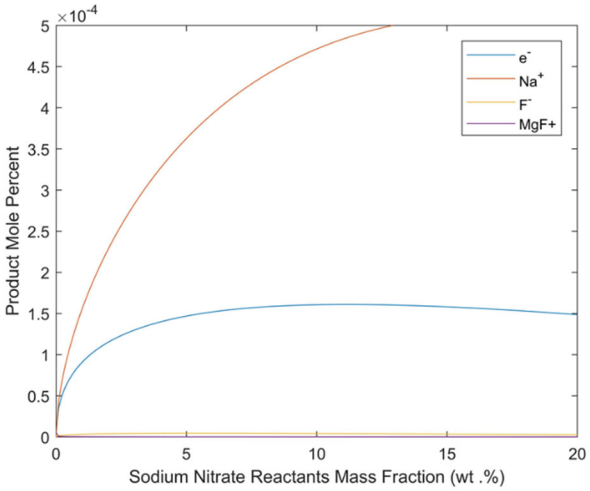

Figure 17. CEA simulation of a 1/1 wt. ratio Mg/PTFE pyrotechnic with addition of $NaNO_3$.

Similar to experiments ran in the multimodal cavity, microwave enhancement of flame emission volume and color is observed. As seen in Fig. 18, images with and without a microwave field (~30 kV/m, WR-284 open waveguide, 2 kW power) are shown for the four formulations exploring the effects of free electron concentration. Each formulation varies throughout time, as a microwave plasma couples with hot products and continues to deposit energy until this region advects out of the field. However, variation in both color and emission can be seen in the image montages. The case with the lowest free electrons (0 wt.% $NaNO_3$), the microwave plasma appears to be sporadic in time, and the region of plasma emission can be observed to continue to emit as it advects away from the burning surface. Instances in time where there is no microwave enhanced luminosity also can be observed. This time instability appears to be mitigated by addition of 0.1 wt.% $NaNO_3$ dopant. Moreover, increasing $NaNO_3$ concentration affects color emission, as Na atoms is more readily available to deposit microwave energy and produce emission mainly due to the Na D line (589nm). Blue emission features seen in most of the formulations is expected to be caused by MgO green bands.

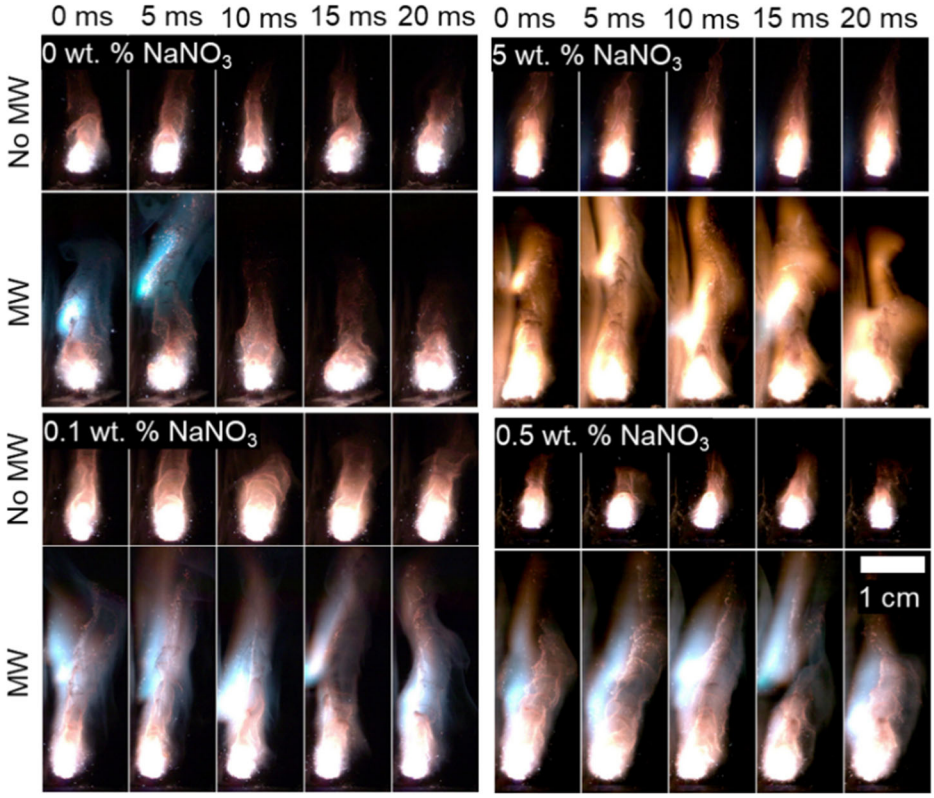

Figure 18. Color image sequences of the combustion plume from Mg/PTFE doped with indicated quantities of $NaNO_3$. Combustion occurs within a free space microwave field with application of field (bottom) and without field application (top). Images are all taken with the same exposure (10 μs) and aperture settings. The free space field was generated from an open waveguide with a 2 kW magnetron.

From these results, microwave enhancement of light emission of the UV/VIS/NIR was observed. The time-integrated spectra of all formulations combustion with and without a microwave field is shown in Fig. 19. Microwave interactions with the flame primarily enhanced molecular and atomic electronic transitions, with little condense phase enhancement observed. These molecular electronic enhancements included MgF/MgO/Mg UVA bands, MgO green bands, and MgF UVC bands, while atomic emission enhancement included Na bands. As for formulations, $NaNO_3$ appears to affect emission enhancement of these molecular/atomic bands, and with increasing $NaNO_3$ concentration up to 0.5 wt.%, these emission features are optimized. However, with further doping, molecular band emission decrease, while condense phase emission is observed to increase slightly. It is expected that addition of a small quantity of alkali nitrate is able to favorably enhance blue/green emission without adversely affecting the color through promotion of the free electron population within the flame and enhanced collisional energy transfer with MgO species.

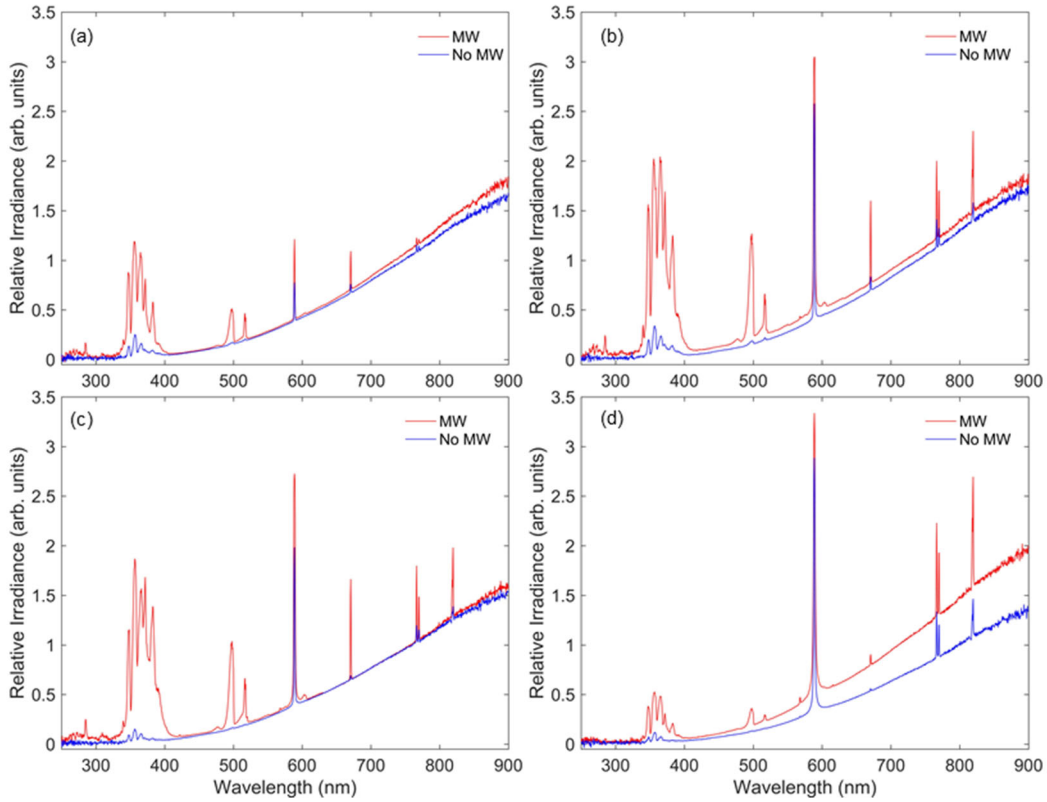

Figure 19. Total integrated emission of 1/1 wt. ratio Mg/PTFE pyrotechnic expose to a microwave field as a function of $NaNO_3$ addition. a) 0 wt.% $NaNO_3$, b) 0.1 wt.% $NaNO_3$, c) 0.5 wt.% $NaNO_3$, d) 5 wt.% $NaNO_3$.

Typical emission from a Mg/PTFE pyrotechnic plume is dominated by the condense phase emission. This can be seen in Fig. 20, where combustion without a field (black) follows the curve of a black body emitter (blue dash line). When Mg/PTFE combustion is exposed to a microwave field, a slight shift in chromaticity is observed, as seen in Fig. 20 (cyan). This resulting shift in color is many due to the electronic excitation of the MgO green bands, which is the main visible range molecular transition that is enhanced. *These findings, taken together, suggest that 1) time instabilities in light emission are observed in formulations with low electron populations (e.g. neat Mg/PTFE); these instabilities appear to be related to the advective features of the flame and can be damped out through addition of a small quantity of alkali, 2) addition of a small quantity of alkali can promote emission from weakly emitting molecular flame species such as MgO, and 3) in higher quantities of addition, alkali dopants can drastically change the flame color to be more similar to that of the neat alkali emitter.*

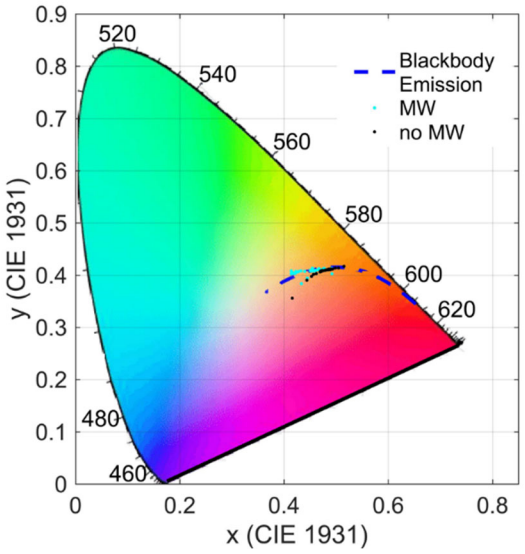

Figure 20. CIE 1931 color space diagram of a 1/1 wt. ratio Mg/PTFE with 0.1 wt.% $NaNO_3$ addition. Blue dash line represents a black body emitter from 1000K to 5000K.

Effect of Variation of Mg/PTFE Stoichiometry on Emission in a Free-Space E-Field

From previous results of Mg/PTFE combustion in the multimodal cavity, diffusion flame structure appeared to have a significant effect on microwave color/flame emission. Within this study, Mg/PTFE combustion stoichiometry was varied to investigate effects on microwave color and emission intensity. Three different formulations were investigated in the free space cavity under a ~30 kV/m field, including formulations of (1) 35/65 wt. % Mg/PTFE (near stoichiometric conditions), (2) 50/50 wt. % Mg/PTFE (fuel-rich combustion), and (3) 65/35 wt. % Mg/PTFE (more fuel-rich).

Color imaging of two of the Mg/PTFE formulation flames can be seen in Fig. 21. Only the two most fuel rich formulations were able to couple with the microwave field. For the near-stoichiometric condition (images not shown), little visible emission enhancement was observed, which can be seen in the time-integrated emission spectra in Fig. 22. We hypothesize that much of the blue/green emission enhancement from Mg/PTFE pyrotechnics is a result of MgO species produced from Mg/air diffusion flame features which locally, are higher flame temperature than the bulk flame. The presence of Mg/air flames in a fuel lean condition are significantly reduced. For the fuel-rich cases, the 65/35 wt. % Mg/PTFE pyrotechnic was observed to have higher molecular/atomic emission. This can be seen in Fig. 22, where both the UVA band (MgO/MgF/Mg) and the MgO green band are enhanced with the microwave field.

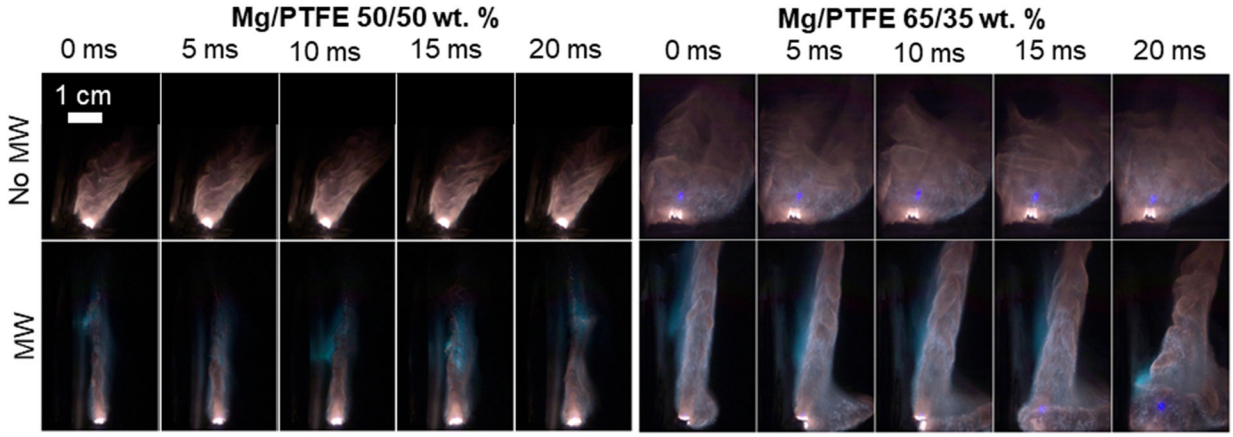

Figure 21. Color images of Mg/PTFE combustion within a free space microwave field (bottom) and without a field (top). Images are taken with the same exposure (10 µs), aperture settings, and a neutral density filter (OD 1.2). The free space field was generated from an open waveguide with a 2 kW magnetron.

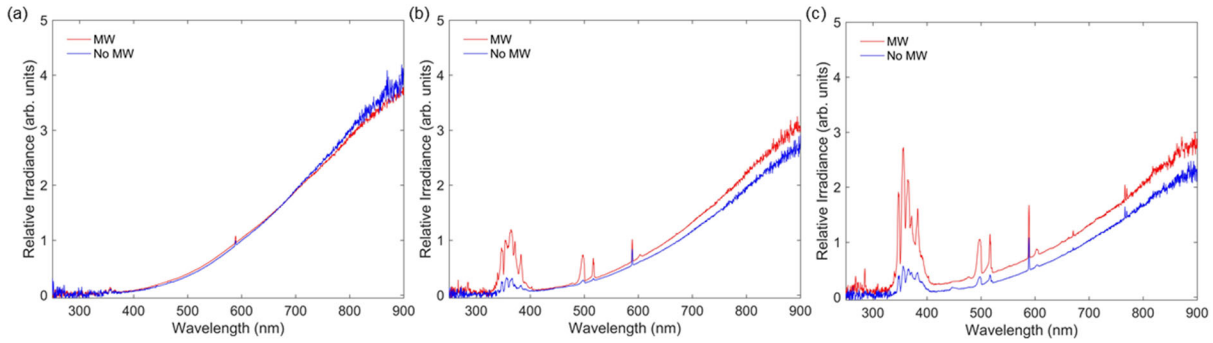

Figure 22. Emission spectra of Mg/PTFE combustion with and without a microwave field (free space field). Formulation are the following: (a) 35/65 wt. Mg/PTFE, (b) 50/50 wt. Mg/PTFE, and (c) 65/35 wt. Mg/PTFE.

To understand microwave energy transfer to magnesium particle flame features, high-resolution emission spectra were captured from burning Mg/PTFE pyrotechnics and simulated emissions spectra were temperature fitted to the experimental spectra. In order to collect light from the $B^1\Sigma - X^1\Sigma$ ($\Delta v=0$) transition of MgO during combustion of Mg/PTFE pyrotechnics, a benchtop spectrometer (Andor Shamrock 500i) with a 300 line/mm grating and a charged-couple device (CCD, Andor Newton DU940) detector was used to image flame emission. A 50 mm diameter plano-convex lens was utilized to image flame emission onto a fiber (Thorlabs M74L05, 400 µm, 0.39 NA). To measure the instrument function of the dispersive spectrometer, a single-mode Coherent Verdi laser at 532 nm was used to illuminate the optical fiber and match the optical path of the experiments. The instrument function is modeled as a Gaussian fitted to the experimental measurement of the laser linewidth (17.5 cm^{-1}). The estimated field strength at the location of the pyrotechnic in these experiments is ~30 kV/m. The emission was modeled with PGOPHER. A non-linear optimization routine was implemented in Matlab using the patternsearch algorithm using only emission spectra with a signal to noise ratio of over 20 (SNR = Peak Signal / Standard deviation of background). An example of the MgO emission spectra fitted to the model is shown in Fig. 23.

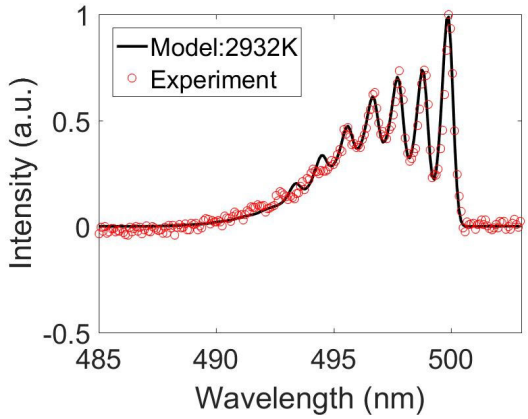

Figure 23. Example fitting of MgO $B^1\Sigma$ -$X^1\Sigma$ ($\Delta v=0$) emission spectra and temperature fitting of the simulated transition.

Gas-phase temperature fitting of MgO was conducted for experiments both with and without microwave field application for the two fuel-rich formulations. Spectra acquisitions were taken during the combustion period of pyrotechnic samples and temperatures were fitted to each spectra and MgO temperatures over the duration of a burn were binned. Spectra from ignition and extinguishment transients were omitted from this analysis. The results of these binning calculations are shown in Fig. 24. It was found, in both formulations, the MgO temperature is increased by MW field application by ~100 K. For the 50/50 wt. ratio Mg/PTFE pyrotechnic, a bimodal temperature distribution was observed and temperature enhancement was highly periodic over the pyrotechnic burn duration. The bimodal MgO temperature distribution and periodic temperature enhancement are further indicative of periodic microwave coupling to the flame over the duration of a pyrotechnic burn, which is consistent with periodic emission color shifting observed in other experiments in both free-space and multimodal cavities. It is expected that periodicity is a result of the microwave field coupling with hot products and continued microwave energy deposition to hot products until this region advects out of the E-field. Bimodal temperature distributions may also be a result of local flame temperatures being limited by the thermodynamic phase change of MgF_2, which occurs at ~2533 K.

In summary, and consistent with studies on alkali doping discussed in the previous section, these findings suggest the presence of periodic coupling within weakly ionized pyrotechnic plumes and emphasize the importance of advection in coupling and energy transfer. Measurements of MgO temperature within pyrotechnic plumes are evidence of microwave energy deposition to MgO species, and molecular temperature fitting is demonstrated as a unique tool to quantify species energy transfer.

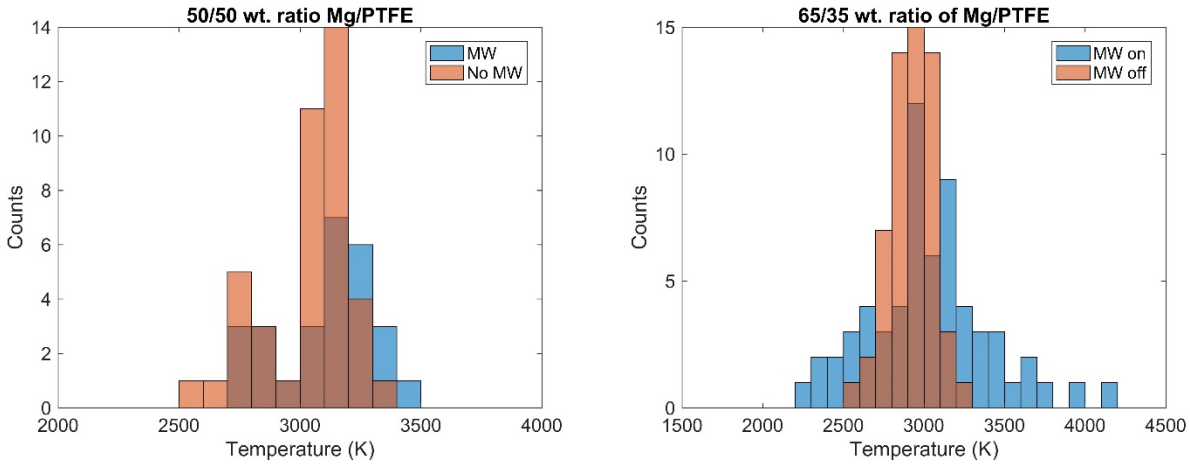

Figure 24. MgO rotational-vibrational gas-phase temperatures of Mg/PTFE combustion (50/50 wt. ratio left, 65/35 wt. ratio right) with and without microwave from two pyrotechnics experiments within a 2.45 GHz free-space microwave field of 30 kV/m.

Plasma Modeling Using Monte-Carlo Methods

The widely available techniques for solving the electron Boltzmann Equation, such as BOLSIG+, typically rely on several critical assumptions that may not be appropriate for application to electrons in atmospheric gases. These include (1) assuming that the time-dependent electron momentum distribution is nearly isotropic (two-term approximation), and (2) that portions of the energy distribution do not vary with time while others are time-independent. To test these assumptions, BOLSIG+ was compared against Monte Carlo simulations across the axial length of a representative premixed methane flame. Simulations of 1D steady flames were obtained using the Cantera software, with the axial flame temperature and mixture used as inputs to Monte Carlo and Bolsig+. The local reduced microwave field strength and frequency were determined from an applied frequency and field strength, divided by the local total gas density. Reaction rates and average electron energy were collected and compared at a series of points within the flame, representing cool reactants and hot combustion products.

The results demonstrate a significant discrepancy between BOLSIG+ and Monte Carlo simulations, which strongly suggests the time-independent EEDF assumption in the BOLSIG+ solver cannot accurately capture time-dependent behavior present in atmospheric combustion conditions.

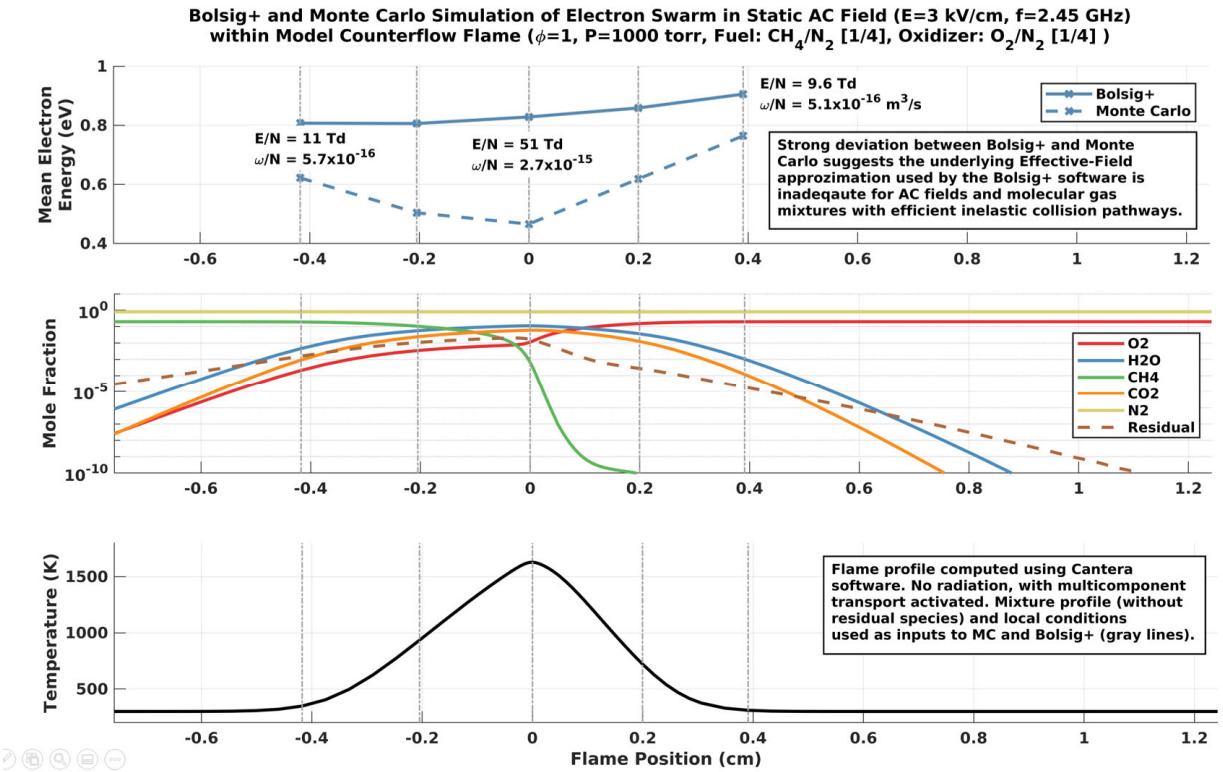

Figure 25. BOLSIG+ and Monte Carlo predictions of mean energy across a representative methane-air flame. Axial mixture and temperature were computed using Cantera.

Modeling of the Microwave Enhancement of Light Emission from a Mg/NaNO3 Pyrotechnic Flame

Using the recently developed 1-D model of pyrotechnic combustion and light emission with illumination by an electric field, this portion of the effort revisited the results of microwave emission enhancement experiments conducted on Mg/alkali nitrate pyrotechnics within a multimodal cavity in order to 1) demonstrate the model's validity in predicting the degree of microwave-induced light emission enhancement observed as a function of alkali dopant type (one of Cs, K, or Na), 2) explain fundamental phenomena both limiting and leading to high degree of light emission enhancement, and 3) to predict conditions of optimum degree light emission enhancement.

In order to compare the proposed model to experimental results, integration of the spectral irradiance from 400 to 880 nm in Fig. 26 was used to produce an estimate of the ratio of time-integrated irradiance with and without microwave exposure (green dots, Fig. 26a). Surprisingly, this emission enhancement was found to correlate positively with shorter wavelength, higher energy, transitions. The pyrotechnic with the highest alkali transition energy, $NaNO_3$, yielded a ratio of 2.2, or 120% increase in time-integrated irradiance when microwaves were applied. Potassium and cesium cases experienced an average of 50% and 20% irradiance enhancements, respectively. These results were compared directly to simulated ratios of radiance computed using Eqn. 14.

Given the challenges in grounding simulation parameters (gas temperature T_0, field strength E_{RMS}/n_{amb}, and alkali mole fraction X_{alk}) firmly in measurements, we instead show that a suitable parameter set exists that can replicate all three alkali enhancement ratios simultaneously. Such a case was found for reduced field strength of 42 Td, plume temperature of 2725 K, and an alkali fraction of 6 vol.%, and is within experimental margin of error for all alkali species (blue dots, Fig. 26a). This serves as an initial demonstration of consistency for the WMIP model for pyrotechnic emission enhancement. For comparison purposes, we also present calculations for the same case but with a gas temperature near CEA equilibrium temperatures (red dots, Fig. 26a).

As the reliance of Eqn. 14 on wavelength (or transition energy) could not be obtained by simple inspection of Eqn. 4-13, the various wavelength dependencies within the model were artificially perturbed from line center λ_{21} to identify the dominant terms (solid and broken lines, Fig. 26a). To simplify the results, wavelength parameters λ_- and λ_+ were used to group terms with similar effects on emission enhancement. Specifically, the λ_- group followed the experimental trend of diminishing enhancement with increasing wavelength, whereas λ_+ opposed it. From initial calculations, it was immediately clear that only the wavelength dependence of K_{M+} (Eqn. 9) contributed to λ_-. The λ_+ term contained all other wavelength dependencies, including: (1) calculation of transmittance via optical depth (Eqn. 5), (2) spontaneous emission coefficient (Eqn. 6), and (3) cross-sections for electron-alkali excitation, where cross-section curves were artificially shifted in energy space to correspond to an alternate transition energy ($\Delta\epsilon = hc/\lambda_+$). The procedure for altering cross-sections does not account for hypothetical changes in cross-section shape, however the curves are roughly comparable across alkali species, independent of transition energy. Finally, both λ_+ and λ_- were also varied together to show the cumulative sensitivity to wavelength.

With the results displayed in Fig. 26a, a preliminary hypothesis can be constructed to explain why WMIP emission enhancement in the VIS/NIR range is maximized for alkali species with shorter wavelength (higher-energy) transitions. Photons with shorter wavelengths (Eqn. 5) have a diminished probability of escape, which restricts the effect of any enhancement. Likewise, alkali species with an increased energy threshold for electron-alkali excitation collisions K_{E+} plainly counters the ability of an electric field to promote non-equilibrium emitters. The same can be said for emission coefficient, which increases the baseline emission rate independent of the microwave field by the third power of wavelength (Eqn. 6). Despite these effects, the model for enhancement is most sensitive to neutral-alkali excitation rate K_{M+} (Eqn. 9), which falls off exponentially for transition energies above the gas thermal energy ($hc/\lambda > k_b T_0 \approx 0.25$ eV). The net effect is that K_{M+} falls off faster with lower wavelength than K_{E+} (whose rate is field-driven and not limited by equilibrium Maxwell-Boltzmann statistics). Hence, K_{E+} develops a proportionally larger effect than K_{M+} on emitter population N_2 (and hence, emission rate ϵ) through Eqn. 7.

To further reinforce that this result is independent of parameter selection, simulations at line-center wavelength were conducted across a wide domain of parameter space ($T_0 = [2400, 3000]K$, $X_{alk} = [0.05, 0.2]$, E_{RMS}/n_{amb},=[20, 45] Td), and the eight combinations were

plotted in the background of Fig. 26a. These show that the general trend between the alkalis hold for all but one case. The extraneous limit with very low enhancement was a result of strong shielding properties ($T_0 = 3000\,K, X_{alk} = 0.20,\ E_{RMS}/n_{amb}$,=20 Td). To show the parameter space in more detail, the intensity ratio solution computed in Fig. 26a for sodium was expanded in Fig. 26b over a broad range of temperature and field strength values (matching the above limits, but with $X_{alk} = 0.06$). Contours representing the experimental mean and standard deviation are shown, identifying a locus of temperature and field strength values that provide high-quality fits. This demonstrates that the enhancement for sodium is consistent with relatively weak microwave fields (<30 Td), provided the plume temperature is significantly lower than equilibrium temperature ($T_0 \ll 3000\,K$). This is also consistent with the intense enhancement observed during the cool post-combustion time period shown in Figure 1, where a large reduction in thermal energy, $k_b T_0$, in Eqn. 9 can diminish K_{M+}, a change consistent with a shift to a higher energy (lower wavelength) transition.

While the proposed WMIP model appears consistent with experiments, it is not free of limitations. Most immediate to the wavelength sensitivity analysis, the evaluation of rate coefficients may be incomplete, as: (1) the wavelength dependence of alkali cross-sections are only crudely approximated; and (2) the two-term Boltzmann approximation may carry significant error for high-pressure molecular discharges. These limitations require further review. For the model, the lack of a well-prescribed temperature distribution, field strength, and alkali mole-fraction prevents rigorous validation, and the homogenous plume assumption must be tested against spatially-resolved temperature and radiance data. These limitations reinforce the need for further investigation with more capable numerical methods and improved diagnostics.

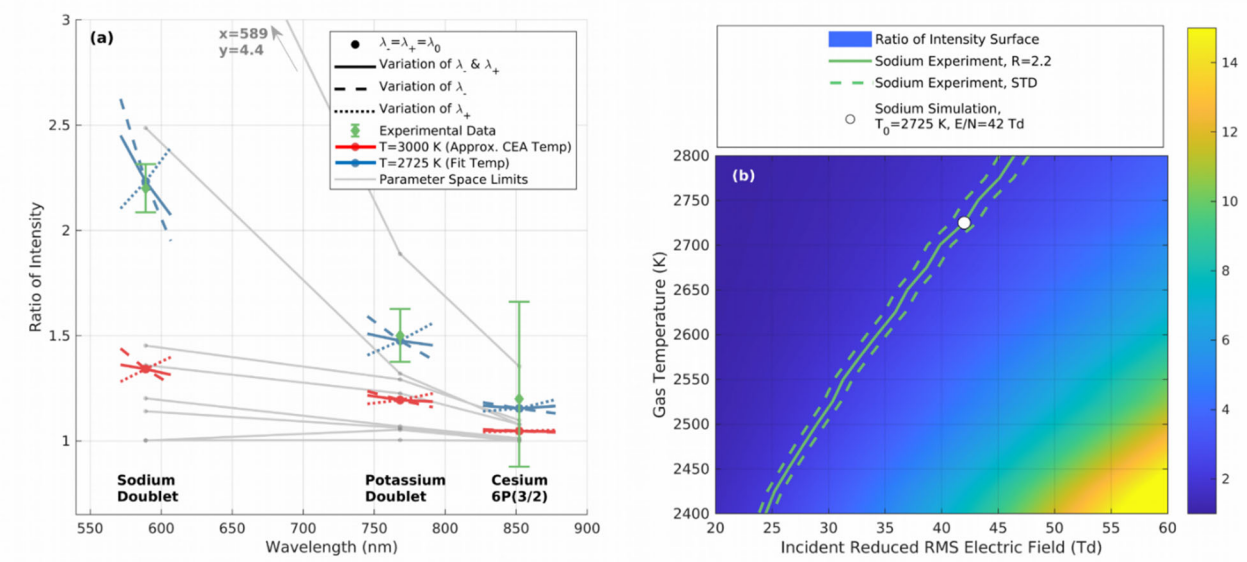

Figure 26. (a) Model results for ratio of radiance with and without applied microwave is shown (Eqn. 14). A best fit solution was found for incident RMS field strength of 42 Td, alkali mole fraction of 6 vol.%, and temperature of 2725 K (blue). A high temperature case representative of CEA equilibrium conditions is also shown (red). Each case is plotted at line center λ_{21}, with perturbations in wavelength showing the local sensitivity from several terms in Eqn. 3-15 producing positive change with wavelength (λ_+) , the single term K_{M+} producing negative change (λ_-), and total change (λ_- and λ_+). Experimental frequency-integrated irradiance ratios are also plotted, with error bars representing the standard deviation of three trials (green).

Lastly, a set of eight simulations are shown covering the practical limits across the three major parameters (gray). (b) The enhancement ratio in (a) is computed for sodium over a range of temperature and field strength values. Contours representing the corresponding experimental value plus/minus one standard deviation are overlaid with simulations, along with the fitted temperature and field strength.

In summary, this investigation demonstrates the numerical model's capability to accurately predict the degree of light emission enhancement occurring from E-field interaction with an alkali-containing plume. Contrary to intuition, the model presents strong evidence that greater degrees of light emission are achieved with alkali species and transitions thereof occurring at lower wavelength (higher energy). Investigation of varying field strength and flame temperature suggest that conditions of high field strength and low flame temperature could yield degrees of emission enhancement nearly an order of magnitude greater than that of the current experimental conditions (i.e. emission enhancements on the order of a factor of 10).

Microwave Interaction Barium Nitrate-Doped Mg/PTFE Pyrotechnics in a Free-Space E-Field

The potential for light emission (brightness and color) enhancement of Mg/PTFE/$Ba(NO_3)_2$ pyrotechnics in a free-space E-field was investigated. Traditionally, barium based pyrotechnics utilized a chlorine donor, in the form of polyvinyl chloride (PVC) to produce the green emitter molecular species, BaCl. However, as a first step toward understanding microwave interaction with such a formulation containing a chlorine donor, we have investigated BaF molecular transitions (in absence of chlorine) by adding small amount of $Ba(NO_3)_2$ (5 wt.%) to 1/1 wt. ratio of Mg/PTFE. Both spectra emission and chromaticity can be seen in Fig. 27 and Fig. 28. Emission enhancement of the BaF transitions can be seen, along with the UVA bands of MgO/MgF/Mg and green bands of MgO/Ba/Mg. Unlike BaCl emission, BaF emits in the far visible red to NIR range (670-940 nm). This results in no chromaticity shifting towards the red region, due to BaF emission being a region of low ocular efficiency.

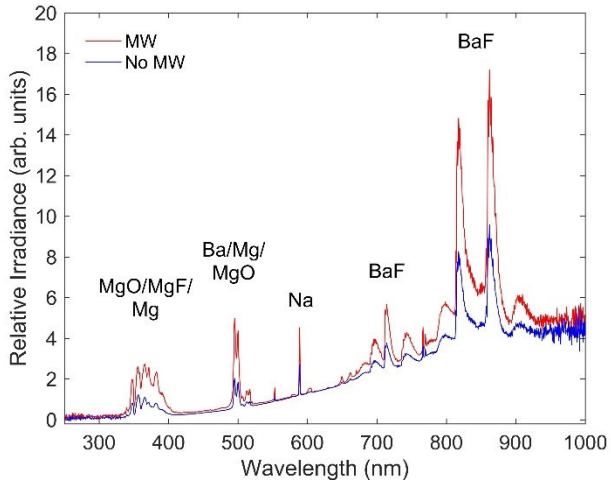

Figure 27. Emission spectra of 47.25/47.25/5 wt. % Mg/PTFE/$Ba(NO_3)_2$ combustion with and without a microwave field (free space field).

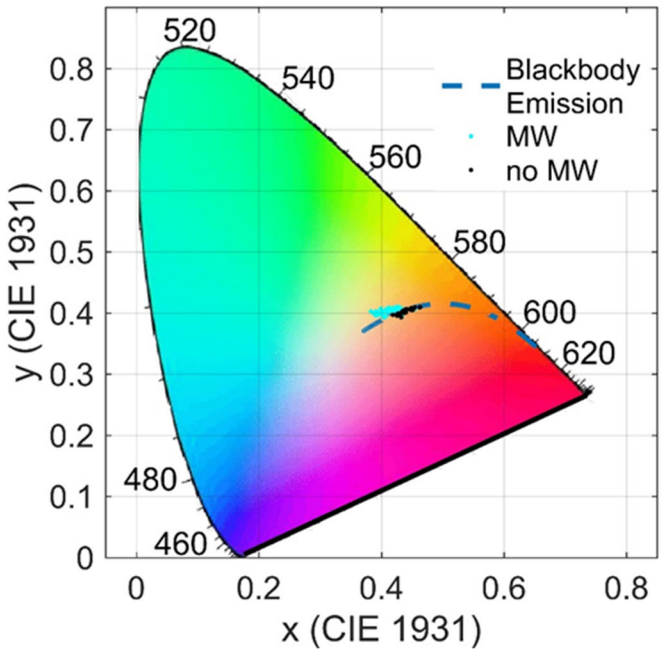

Figure 28. Chromaticity diagram showing dominant emission color of $Ba(NO_3)_2$-doped (5 wt.%) Mg/PTFE pyrotechnic flames both with and without microwave illumination. Microwave illumination is from a 2 kW magnetron source within a free-space cavity.

Boron Combustion

This study focused on characterizing the microwave enhancement of boron combustion within a fuel-rich solid propellant based on burning rate, condensed-phase temperature, and molecular emission. These results are demonstrative and instructive to efforts to microwave modulate the light emission from boron-containing pyrotechnics. In this study, the effects of boron loading (10 wt.%, 20 wt.%, and 30 wt.%) within the propellant were analyzed and propellants containing boron were compared to those containing boron carbide, which unlike boron, is known to absorb 2.45 GHz efficiently through dielectric modes, as it is frequently used as a microwave coupling additive and is manufactured into bulk parts through industrial microwave sintering.

Microwave irradiation was found to significantly enhanced both molecular BO_2 and continuum emission for all propellant loadings of boron and boron carbide except for the propellant containing 30 wt% boron carbide. Equilibrium predictions of adiabatic flame temperature indicate that flame temperature decreases with increased loading of boron, due to a decreasing oxygen balance, which is expected to be the source of decreased continuum emission with increased metal content (not shown). Microwave application increases both the underlying continuum emission and molecular BO_2 emission in the 450 – 600 nm band (Fig. 29a). Both BO_2 emission (Fig. 29b) and total emission (Fig. 29c) show that microwave emission irradiation results in increased emission with increasing metal content. Without microwave irradiation, increasing the metal content decreases both BO_2 emission and total emission with both boron and boron

carbide fuels. With microwave irradiation, both BO_2 emission and total emission are reduced only slightly with increasing boron content, and as a result, the degree of both BO2 and total emission enhancement drastically increases with increasing addition of boron to the propellant. A more modest increase in emission is observed in microwave irradiated boron carbide propellants and no obvious trends are seen with regards to metal loading. Without microwave application, boron carbide propellants exhibit BO_2- emission features similar to boron propellants but do not produce the same levels of emission enhancement as a result of microwave irradiation. The lack of appreciable light emission enhancement observed in boron carbide containing propellants as a result of microwave irradiation suggest that microwave energy transfer by dielectric means to a reactant species is not a favorable method through which to enhance pyrotechnic light emission.

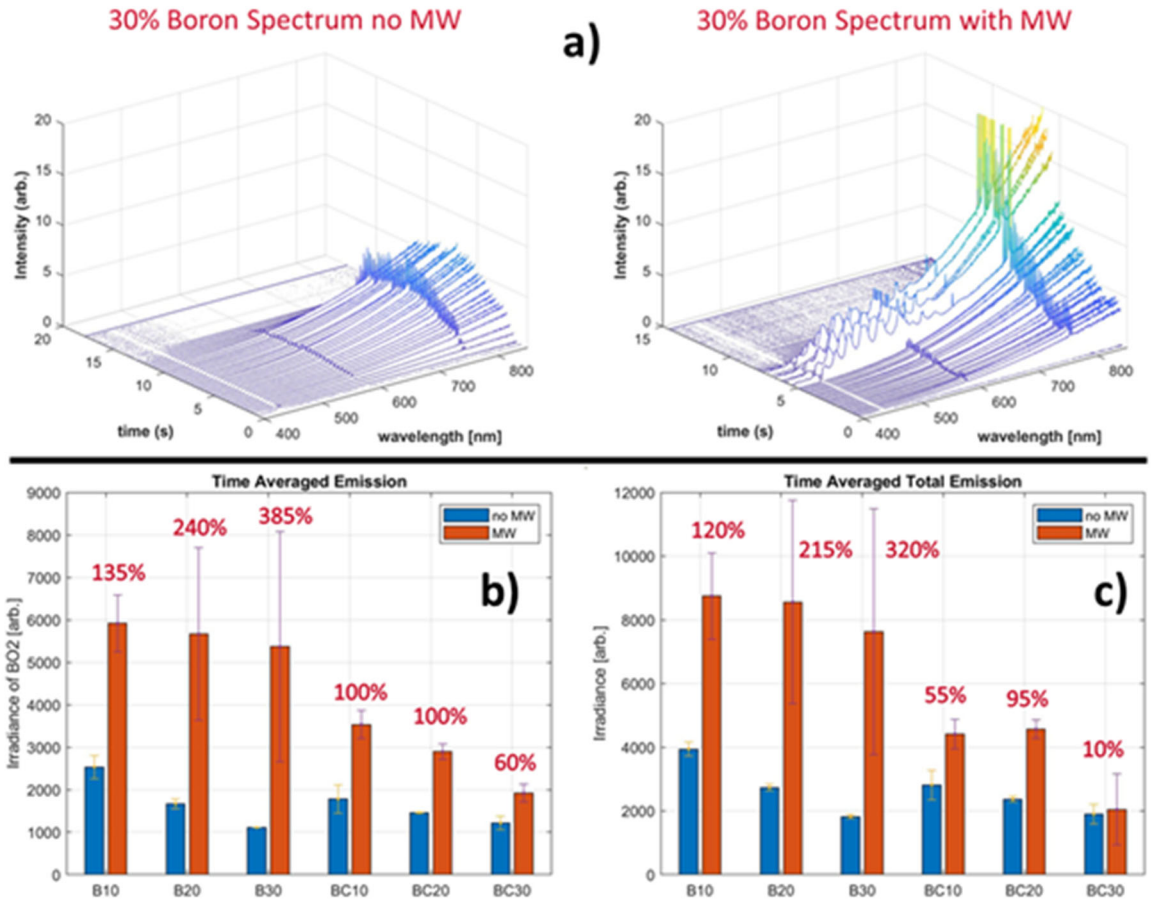

Figure 29. a) Time-resolved spectra of a 30 wt% boron propellant without (left) and with (right) microwave irradiation. b) Time-averaged BO_2 emission and c) time-averaged total emission(400 to 850 nm) for boron (B) and boron carbide (BC) propellant formulations both with and without microwave irradiation. Percentages indicate the degree of emission enhancement as compared to the same formulation without MW.

Microwave enhancement of propellant burning rate was found to be higher for boron carbide propellants while only one of the boron propellants showed a significant increase in burning rate (Fig. 30). Without microwave irradiation, the burning rate of boron carbide propellants decreases with increasing metal loading, both with and without microwave irradiation. This trend was not observed in boron containing propellants, however, and with increasing boron

content, the burning rate of boron propellants without microwave irradiation remained relatively unchanged. Microwave irradiation resulted in a small increase in burning rate of propellants containing 10 wt.% and 30 wt.% boron but resulted in a 40% increase in burning rate for propellants containing 20 wt.% boron. The source of this high degree of mi

Boron loaded propellants had similar or higher burning rate when compared to boron carbide propellants with or without microwave application. Interestingly, boron propellants did not show significant burning rate enhancement for 10% or 30% loadings but showed the largest enhancement and highest overall burning rate for 20 wt% boron loading. This may indicate an optimal loading at 20 wt% boron but the cause for the high burning rate remains unknown and further experimentation and analysis would be required to validate and understand this finding.

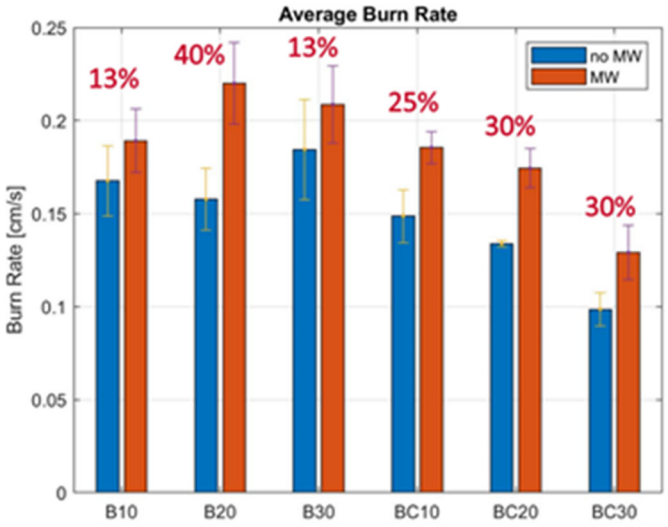

Figure 30. Average burning rate across three trials for each formulation. Enhancement due to microwave irradiation shown in percent above each formulation. Error bars indicate one standard deviation of all measurements.

The degree of flame temperature enhancement occurring as a result of microwave irradiation was measured through fitting of visible wavelength emission spectra to a graybody continuum according to the procedure described in the methods section. As such, the temperatures reported in this study are highly biased toward the condensed phase reactant and product species within the flame (e.g. boron, boron carbide, condensed phase products thereof, and carbonaceous species). Temperatures measured during the duration of a burn were averaged for each formulation and microwave condition and are shown in Fig. 31. These results show that flame temperature is primarily affected by formulation and microwave irradiation had no effect on measured temperature. Condensed-phase temperatures for all formulations were observed to range from 1900 - 2100 K. The absence of microwave temperature enhancement, combined with the strong enhancement of continuum emission is expected to be a result of the volatilization temperature limit of boron trioxide (2133 K), suggesting continuum temperatures in boron and boron carbide propellants are highly biased toward this species. Despite this thermodynamic limit that hampers measurement, it is expected that some microwave energy is transferred to the condensed phase product species. The higher continuum emission observed in spectra as a result of microwave irradiation (Fig. 29a) is expected to be a result of higher burning rate.

Overall these results indicate that, in a propellant combustion environment, boron carbide does not produce favorable degrees of microwave-induced light emission enhancement—evidence against the effectiveness of incorporating reactants with strong dielectric absorption as a means of enhancing light emission. However, the degree of light emission enhancement from boron formulations (up to 385%) is promising and suggests that boron combustion (through microwave interaction with BO_2 species) should be considered and further studied as a means through which to amplify light emission.

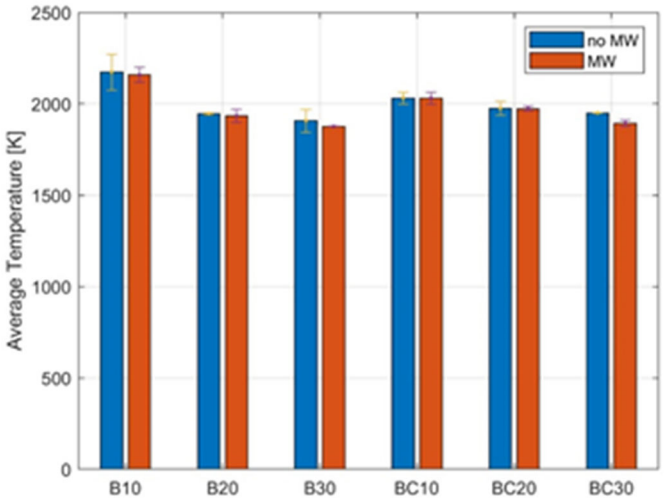

Figure 31. Computed graybody temperature measurement from propellant flames with and without microwave irradiation. Values are averages and error bars indicate one standard deviation of all measurements.

Development of Gas-Phase, Premixed Particle-Seeded Burner for Microwave Interaction Studies

A gas-phase, premixed burner capable of flame seeding by either solid particles or by atomized suspensions of alkali salt solutions was developed in order to enable experimental measurements with greater repeatability, longer test durations (resulting in greater statistical significance), and greater control over conditions in order to more carefully study mechanisms of microwave enhanced combustion and provide data more suitable to comparison with experiment. Images of the burner in operation without seeding and with solid particle seeding are shown in Fig. 32. Once designed and manufactured, the burner was tested using ethylene and air to determine flammability limits and stability. Initial testing determined that the burner could maintain a flame down to a ~ 0.8 equivalence ratio (φ) at a flow rate of ~5 SLPM. Most favorable flame conditions were observed at φ= 1.8 using a 6.75 SLPM total flow rate (6.0 Air, 0.75 SLPM C_2H-4) or a 14.1 SLPM total flow rate (12.5 Air, 1.6 C_2H_4). These conditions offered the best combination of a tall flame and stability. The adiabatic flame temperature for ethylene and air is predicted at φ = 1.2 but this did not result in an optimal flame height for particle combustion and appeared fuel rich during testing, which may indicate that the gases are not perfectly mixed prior to exiting the burner. The testing was accomplished both with and without the glass beads to determine their effect on flame stability and mixing but no significant difference was found between the two cases. Therefore, the

beads were included in all future testing as a means to safely reduce the volume of the gas within the burner to improve safety in the event of a flashback.

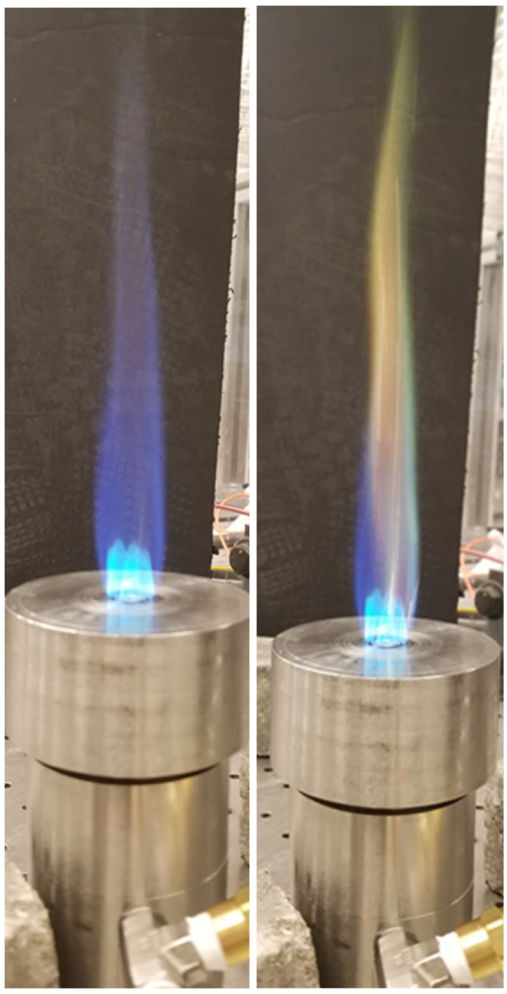

Figure 32.Image of premixed particle-seeded gas burner stable flame condition without seeding (left) and with boron particle seeding (right).

Initial testing was done with the particle feeder to determine the appropriate settings for the feeder screw speed, particle loading of the screw, and entrainment gas flow rate. A prescribed mass of particles is brushed onto the screw threads and the screw is then placed inside the brass tubing. The screw is then rotated by hand or using a more precise position-controlled DC motor. Particle entrainment was achieved at less than 1 SLPM and single particle combustion was observed with both aluminum and boron particles with ~1 mg of metal loading. Testing and characterization of the spray atomizing seeder was not completed by the conclusion of this one-year effort due to long delays in acquisition of the spray atomizer (TSI Corp), which is currently in high demand for use in generating aerosols for study of COVID-19 transmission.

Flame temperature measurements of the burner were made using both 2-color pyrometry and graybody curve fitting of emission data. Calibration of flame temperatures for the premixed

ethylene flames was not completed by conclusion of the one-year effort, though preliminary calculations indicate flame temperatures match well with equilibrium predicted adiabatic flame temperatures, though there is concern that flame temperatures and particle residence times within the flame may not be sufficient for ignition and combustion of some metal fuels(e.g. aluminum and boron). Future efforts should focus on use of the burner with higher flame temperature acetylene-air flames and analysis of combustion of both alkali metals as well as metal particles.

Conclusions, Future Research Directions and DoD Implications

This effort has 1) demonstrated the microwave enhancement of flames from a number of pyrotechnic formulations in a free-space microwave field of 2.45 GHz frequency, 2) led to the development of a suite of modeling tools capable of predicting the degree of light emission enhancement occurring from microwave-flame interaction and providing insight into fundamental light emission mechanisms and enhancement, and 3) has led to the development of a particle-seeded burner to be used in studies of microwave enhancement of light emission. Following are more specific findings of significance on topics explored by this effort.

Effect of free electron concentration on alkali-doped Mg/PTFE in a free-space microwave field.

Addition of up to 5 wt.% of an alkali additive (i.e. sodium nitrate) to a Mg//PTFE pyrotechnic in order to increase the free electron concentration of a flame has been demonstrated as an effective technique to damp out time instabilities in microwave color switching of such compositions that are observed in both free-space and other microwave cavities. Low level dopant addition (0.5 to 1.0 wt.%) also improves the energy transfer to MgO species responsible for color switching. When an alkali dopant such as sodium nitrate is added at higher concentrations (5 wt.%), microwave illumination effects are switched from those similar to a formulation with weakly ionized flame species (e.g. flame color switching observed from MgO species in Mg/PTFE) to those of a formulation with highly ionized flame species (e.g. light amplification observed in $Mg/NaNO_3$) and drastic amplification of luminosity and flame volume are possible with microwave modulation. Separate investigations were conducted on barium nitrate-doped Mg/PTFE pyrotechnics (5 wt.% $Ba(NO_3)_2$). The eventual goal of studies on barium additives is the study of barium chloride green light emission augmentation. However, as a first step, formulations are tested in the absence of a chlorine donor. In studies on $Ba(NO_3)_2$-doped Mg/PTFE, it was observed that microwave irradiation amplifies luminosity of the formulation and produces a slight chance in chromaticity. These findings suggest that many different light emission profiles may be possible from a single ‘base’ pyrotechnic formulation doped with small quantities of additives; such a technique would simplify pyrotechnic manufacture and might reduce reliance on environmentally harmful pyrotechnic additives. The results presented herein suggest that such a technique might be successful for a number of formulations, though optimization of E-field conditions and optimization of a ‘base formulation’ to which to add dopants should be addressed.

Effect of variation of stoichiometry on Mg/PTFE emission enhancement in a free-space microwave field.

Formulations of Mg/PTFE with stoichiometries ranging from fuel lean to fuel rich were observed under combustion within a free-space microwave field. Findings indicate that no microwave-induced emission enhanecment was observed in fuel lean formulations. The blue/green light emission (color switching) enhancement produced from microwave-induced energy transfer to MgO species is found to be improved at fuel-rich stoichiometries, no doubt due to the greater prevalence of Mg/air combustion in fuel rich formulations. Measurements of MgO molecular temperature show that microwave irradiation of flames increases the MgO temperature by ~100 K. Combined with studies on alkali doping of Mg/PTFE flames, these results also indicate that coupling of energy to MgO species is time-periodic and related to advection transport of microwave enhanced flame features. These findings demonstrate the imporance of considering species advection and are affirmation of the importance of future modeling efforts to develop spatially resolved simulations on advection timescales. The demonstration of MgO temperature measurement will also, no doubt, serve as a useful technique to diagnose microwave-induced energy transfer to species within flames.

Plasma modeling using Monte-Carlo and two-term modeling methods

A Monte-Carlo solver was developed for solving the Boltzmann Equation directly in order to obtain electron properties for pyrotechnic flame conditions on account of the errors associated with use of the commercially available BOLSIG+ solver for atmospheric pressure conditions. Further expansion of capabilities to 2D and 2D time-transient combustion plumes in order to capture advection effects will likely require, instead of Monte Carlo, two-term solution methods to the Boltzmann Equation to reduce computational overhead of solution.

Mg/alkali nitrate modeling of degree of light emission enhancement

A 1-D, steady state microwave enhanced emission model has been created to predict the degree of light emission enhancement observed from a pyrotechnic plume of high alkali content. The degree of light emission enhancement caused by microwave illumination of pyrotechnic plumes has been compared to the experimentally measured degree of enhancement for three different alkalis (Cs, K, and Na). Model agreement is favorable and leads to a number of important findings. Contrary to intuition, the model presents strong evidence that greater degrees of light emission are achieved with alkali species and transitions thereof occurring at lower wavelength (higher energy). Investigation of varying field strength and flame temperature suggest that conditions of high field strength and low flame temperature could yield degrees of emission enhancement approximately an order of magnitude greater than that of the current experimental conditions (i.e. emission enhancements on the order of a factor of 10). This finding, in consideration of the propensity of fields to selectively couple with high electron populations under advection suggests that combining a short time duration plasma seeding and kernel growth technique with a low flame temperature flame and high strength field may enable sustained, extreme, high degrees of emission enhancement. Additionally, the model developed to predict degree of light emission enhancement is an update to pyrotechnic light emission models developed and infrequently advanced since the 1970s. The model developed in this effort is also relevant to pyrotechnic flame emission in absence of a microwave field and as such is a refresh to a topic if high importance to the DoD. Further efforts in light emission modeling would be fruitful in advancing needed capabilities in pyrotechnic light emission modeling.

Microwave enhancement of light emission from fuel-rich, boron AP composite propellants

Experimental measurements of microwave enhanced light emission were conducted from boron-containing, fuel-rich ammonium perchlorate composite propellants. These emission measurements, while from a propellant formulation, are instructive in that they inform on the ability to microwave modulate green boron trioxide molecular emission. Measurements show that, in a propellant combustion environment, boron carbide does not produce favorable degrees of microwave-induced light emission enhancement—evidence against the effectiveness of incorporating reactants with strong dielectric absorption as a means of enhancing light emission. However, the degree of light emission enhancement from boron formulations (up to 385%) is promising and suggests that boron combustion (through microwave interaction with BO_2 species) should be considered and further studied as a means through which to amplify light emission. The overwhelming degree of green BO_2 light emission enhancement observed from microwave irradiation of fuel-rich propellant plumes suggests high payoff for microwave enhancement of boron-based pyrotechnics and the ability to produce extremely high brightness green pyrotechnics through microwave amplification. Boron based pyrotechnics are a lower toxicity, more environmentally friendly alternative to formulations utilizing barium chloride emission. Additional study is necessary in a pyrotechnic formulation that reduce the degree of continuum light emission.

Development of a premixed, particle-seeded gas phase burner

A premixed, seeded gas-phase burner system and two seeder systems capable of seeding the flame with either solid particles or atomized solutions of alkali salts has been designed and manufactured in order to study, under more controllable conditions, the microwave enhancement of pyrotechnic ingredients. Testing of the system was completed using boron particle seeding. Development of the alkali salt atomization seeder system was delayed by limited supplier part availability caused by COVID-19 and while all parts were received, testing and validation was not completed. Testing has revealed that some modifications to the system would be beneficial for the purpose of studying microwave effects on metal particle seeded combustion. The burner system will also be highly valuable in validation of numerical simulations.

Summary

Overall, this research effort, in particular experimental efforts, were negatively impacted by the COVID-19 pandemic and in the second half of the project, the rate of research progress was reduced. Regardless, results of this one-year effort have, under a number of experimental conditions, demonstrated the ability to extract light emission enhancement (both luminosity enhancement and brightness modulation) from pyrotechnic plumes through microwave illumination in a free-space field environment, effectively mitigating a significant portion of risk associated with future study of the topic. A number of critical, exploratory findings have been made that suggest the potential for high payoff of this research area and are instructive to the direction of future efforts.

It should be noted that for experiments in this study, the 2.45 GHz field strengths used are typically between 10 to 50 kV/m. High-power, focused and targeted microwave sources are currently an area of high research interest and rapid advancement; sources such as these have or are currently being utilized 'in the field.' To maximize impact, efforts in the area of microwave augmented pyrotechnic light emission should be informed of the current state of the art in source capabilities or evaluations conducted with a spatially focused source.

Literature Cited

[1] B.E. Douda, R.M. Blunt, E.J. Bair, Visible Radiation from Illuminating-Flare Flames: Strong Emission Features*†, J. Opt. Soc. Am. 60 (1970) 1116.

[2] J. E. Tanner, A Mathematical Model of Flare Plume Combustion and Radiation, Report No. NWSC/CR/RDTR-9, Naval Weapons Support Center, Crane, IN, USA, 1975

[3] D. R. Dillehay, Resonant Line Broadening of Alkali Metals in Pyrotechnic Flames, [dissertation]. Clayton University; 1983

[4] H. Webster, J.E. Tanner, B.E. Douda, Theoretical Light Yields from Illuminating Flare Compositions, Report No. 253, Naval Weapons Support Center, Crane, IN, USA, 1973

[5] B.E. Douda, E.J. Bair, Radiative transfer model of a pyrotechnic flame, J. Quant. Spectrosc. Radiat. Transf. 14 (1974) 1091–1105.

[6] H. Singh, M.R. Somayajulu, R. Bhaskara Rao, A Study on Combustion Behavior of Magnesium-Sodium Nitrate Binary Mixtures, Combust. Flame. 76 (1989) 57–61.

[7] S.J. Barkley, K. Zhu, J.E. Lynch, J.B. Michael, T.R. Sippel, Microwave plasma enhancement of multiphase flames : On-demand control of solid propellant burning rate, Combust. Flame. 199 (2019) 14–23.

[8] W.H. Sutton, Microwave Processing of Ceramic Materials, Am. Ceram. Soc. Bull. 68 (1989) 376.

[9] Y. V Bykov, K.I. Rybakov, V.E. Semenov, High-temperature microwave processing, J. Phys. D. Appl. Phys. 34 (2001) R55–R75.

[10] H. Fay, The electrical conductivity of liquid Al2O3 (Molten Corundum and Ruby), J. Phys. Chem. 70 (1966) 890–893.

[11] S. Gordon , B.J. McBride , Computer program for calculation complex chemical equilibrium compositions and applications: I. Analysis, NASA Lewis Research Center, 1994 Reference Publication No. RP-1311.

[12] O.B. Laug, Evaluation of A Test Method for Measuring Microwave Oven Cooking Efficiency, Washington DC, 1977.

[13] D. Malacara, Color vision and colorimetry: Theory and applications, Color Res. Appl. 28 (2003) 77–78.

[14] J.J. de Groot, J.A.J.M. van Vliet, The High-Pressure Sodium Lamp, Macmillan Education, London, 1986.

[15] H.W. Drawin, F. Emard, Optical escape factors for bound-bound and free-bound radiation from plasmas Pt 1, Beitraege Aus Der Plasmaphys. 13 (1973) 143–168.

[16] P.L. Lijnse, Electronic-excitation transfer collisions in flames-VI. Interpretation of the temperature dependence of alkali-quenching by N2 and general conclusions about the energy transfer mechanism, J. Quant. Spectrosc. Radiat. Transf. 14 (1974) 1143–1155.

[17] G.J.M. Hagelaar, L.C. Pitchford, Solving the Boltzmann equation to obtain electron transport coefficients and rate coefficients for fluid models, Plasma Sources Sci. Technol. 14 (2005) 722–733.

[18] Biagi database, www.lxcat.net, retrieved on May 1, 2020.

[19] IST-Lisbon database, www.lxcat.net, retrieved on May 1, 2020.

[20] Phelps database, www.lxcat.net, retrieved on May 1, 2020.

[21] K. Igenbergs, J. Schweinzer, I. Bray, D. Bridi, F. Aumayr, Database for inelastic collisions of sodium atoms with electrons, protons, and multiply charged ions, At. Data Nucl. Data Tables. 94 (2008) 981–1014.

[22] K. Ratnavelu, W.E. Ong, Electron and positron scattering from atomic potassium, Eur. Phys. J. D. 64 (2011) 269–285.

[23] O. Zatsarinny, K. Bartschat, N.Y. Babaeva, M.J. Kushner, Electron collisions with cesium atoms-benchmark calculations and application to modeling an excimer-pumped alkali laser, Plasma Sources Sci. Technol. 23 (2014) 35011.

[24] M. Laroussi, Interaction of microwaves with atmospheric pressure plasmas, Int. J. Infrared Millimeter Waves. 16 (1995) 2069–2083.

Appendices

Scientific / Technical Publications

Archival Journal Publications

S Barkley, J Lynch, E Miklasewski, J Dilger, W Crespo, J Michael, S Subramaniam, T Sippel, "Microwave-Assisted Modulation of Light Emission Intensity in Alkali-Pyrotechnic Plumes," *Combustion & Flame*, Under review, resubmitted Sept., 2020.

S Barkley, E Miklaszewski, J Dilger, W Crespo, J Michael, T Sippel, "Microwave Switching of a Magnesium/Teflon Pyrotechnic Flame Color and Intensity," *J. Appl. Physics,* In revision, submitted May 2020.

Conference Presentations/Proceedings

J Lynch, T Sippel, S Subramaniam, "Limitations of approximate Boltzmann solutions for atmospheric combustion with high-frequency electric fields," American Physical Society Division of Plasma Physics Meeting, October 21, 2019, Ft. Lauderdale FL. 2019;2019:JO8-006.